FAST NEUTRON FLUX IN THE UNIVERSITY OF MARYLAND REACTOR

by
Philip Gilbert Berman

Thesis submitted to the Faculty of the Graduate School
of the University of Maryland in partial fulfillment
of the requirements for the degree of
Master of Science
1965

APPROVAL SHEET

Title of Thesis: Fast Neutron Flux in the University of Maryland Reactor

Name of Candidate: Philip Gilbert Berman
Master of Science, 1965

Thesis and Abstract Approved:

Dr. Dick Duffey
Professor
Nuclear Engineering

Date Approved: 19 July 1965

ABSTRACT

Title of Thesis: Fast Neutron Flux in the University of Maryland Reactor

Philip Gilbert Berman, Master of Science, 1965

Thesis directed by: Professor Dick Duffey

The fast neutron flux distribution in the experimental facilities of the University of Maryland Reactor (UMR) was studied by means of neutron activation threshold foils with the reactor at a power level of 10 kw. The foils used were sulfur, magnesium, and aluminum which detected neutrons of energies greater than 3.0 Mev, 6.3 Mev, and 8.1 Mev, respectively. The activities of the foils were measured by calibrated beta and gamma scintillation detection systems. A central row of fuel elements, the west beam port, and the through tube were studied using all three types of foils. The fast neutron flux above 3.0 Mev was measured in each element of the core.

The maximum fast neutron flux above 3.0 Mev available in the central "glory hole" was about $2 \times 10^{10} n/cm^2$-sec. The flux above 6.3 Mev and above 8.1 Mev was about $5.5 \times 10^{8} n/cm^2$-sec and about $4.5 \times 10^{8} n/cm^2$-sec, respectively.

Available in the west beam port was a maximum fast neutron flux above 3.0 Mev of about $2.6 \times 10^{9} n/cm^2$-sec adjacent to the core and of about $1.2 \times 10^{7} n/cm^2$-sec at the inner face of the beam port shield plug.

The fast neutron flux above 3.0 Mev available in the

center of the through tube was 1.7×10^{9} n/cm^2-sec. The minimum at both east and west ends, at the inner faces of the shield plugs, was about 7×10^{5} n/cm^2-sec.

ACKNOWLEDGEMENTS

The author wishes to thank Dr. Dick Duffey whose help and encouragement made completion of this work possible. The author also wishes to thank Mr. P. H. Haas, formerly of the Harry Diamond Laboratories, for his continued encouragement and for allowing the use of equipments of the Laboratories for experimental work associated with this thesis. The cooperation of the Health Physics Office of the Walter Reed Army Medical Center, and particularly of Col. Willis D. Holland and Capt. James Roy of that office, is gratefully acknowledged. The assistance and advice of John Kinch, John Mc Neilly and David Kilminster of the Nuclear Defense Laboratory is gratefully acknowledged. The assistance of Mr. Fred Brittle for operating the University of Maryland Reactor when needed is acknowledged. Finally, the author's wife, whom he really can't thank enough for all she has done - typing illegible manuscripts, keeping the children away and last, but far from least, waking the author at three o'clock in the morning to count threshold detector foils as they decayed away.

TABLE OF CONTENTS

TABLE OF CONTENTS (continued)

TABLE OF CONTENTS (continued)

LIST OF TABLES

LIST OF TABLES (continued)

LIST OF FIGURES

LIST OF GRAPHS

LIST OF GRAPHS (continued)

SECTION I

INTRODUCTION

The desirability of having a well known radiation environment in which to carry out experiments cannot be stressed too greatly. In the University of Maryland Reactor(UMR), the thermal neutron distribution has been carefully studied (1,2) by use of various detectors. However, the fast neutron environment, which is significant in the analysis of many solid and liquid state phenomena, is not so well known.

Reported herein are the neutron fluxes with energy above 3.0 Mev, 6.3 Mev, and 8.1 Mev, respectively. They were determined by the use of threshold-type activation foils using standard evaluation procedures. This technique was necessitated by the presence of fission product decay gamma rays as well as the prompt gamma contribution from the fission process. This detection procedure was originally developed by Hurst, et al. (3), and advanced by the United States Nuclear Defense Laboratories, Edgewood Arsenal, Maryland (4,5,6).

SECTION II

REACTOR DESCRIPTION

A. General

The University of Maryland Reactor(UMR) is a pool-type research reactor. It is fueled with aluminum clad plates of an aluminum-uranium alloy (the uranium being 93.5% U^{235}). The reactor is licensed to operate at a maximum power level of 10 kw.

B. Core

The core (7) is supported by grid plates, fourteen inches above the bottom of the tank. The core has provisions for fifty-four assemblies, either fuel or moderator, in a 6x9 array. However, nine positions are blocked by the through tube; six, by each beam port; one, by the startup chamber and two, by the level safety chamber.

The active lattice is a parallelopiped, 23 5/8 inches high, 12 inches wide, and 12 inches long. There are nineteen fuel assemblies and eleven reflector pieces in the core. Three of the fuel elements have space for the control rods, while two have space in which test items may be placed. One reflector piece has a hole for insertion of the Pu^{239}-Be neutron source, whose emission rate is $1x10^{6}$ n/sec. The source must be in position B-3 for startup and must be removed from the core when the indicated power is about 0.1 watts.

Reflection for the core is provided at the south face

by the thermal column and by the eleven reflector pieces at the east, north, and west faces. See Figure I.

C. Fuel

The fuel elements (8) consist of flat plates of uranium-aluminum alloy, enriched to 93.5% U^{235}. The plates are 26 mils thick, 2.5 inches wide, and 23.625 inches long. The fuel plates, clad on both sides with 27 mils of aluminum, are made seamless by overlapping the clad so that the final fuel plate size is 80 mils thick, 2.7 inches wide, and 25.125 inches long.

The fuel plates are assembled with spacing washers, 0.182 inches thick, interposed between them to provide a center to center spacing of 0.262 inches. See Figure II. The standard fuel element consists of ten fuel plates. However, there are six fuel assemblies which have less than ten plates. Three of the assemblies, in positions C-7, E-4, and E-6, have channels provided for the control rods by removal of the four central fuel plates. Shrouds extend from the rod drive housing to the core in order to protect the rods and their drive shafts from damage or fouling during the placement of experiments. Therefore, access to the fuel assemblies is prevented. Assembly D-5 contains five fuel plates and one solid aluminum buffer plate, providing an experiment irradiation space 2.55x1.625 inches square. Assembly B-5 contains four fuel plates and one solid aluminum buffer plate, providing an experimental space

2.25x1.875 inches square. The fuel assembly in C-4 contains nine active fuel plates and one solid aluminum plate.

All fuel plates, except those in B-5, D-5, and F-8, contain 16±0.2 grams of U^{235}. The exceptions contain 18±0.2 grams of U^{235}. Core loading is nominally 2.671 kgms.

D. Control Rods

Reactor control is accomplished by three control rods, two shim-safety rods, and one regulating rod. See Figure I. The poison sections of the shim-safety control rods are stainless steel tubes filled with boron carbide. The poison section of the regulating rod is merely a hollow stainless steel tube. The poison sections of the rods are 27 inches long. Approximate rod worths are shown in Table I.

TABLE I

Reactivity Worth of the Control Rods

Control rod	Reactivity worth
Regulating	0.358%
Outer Shim-safety, I	2.00%
Inner Shim-safety, II	3.60%

E. Tank

The tank is seven feet in diameter and about twenty-one feet deep (9). Biological shielding consists of 17.5 feet of demineralized water above the active lattice and 2 feet of water plus 7 feet of concrete at the sides of the lattice. The water is circulated at 15 gpm through a heat exchanger,

filter, and demineralizer in order to maintain purity.

F. Beam Ports

Both beam ports (10) are six inches in diameter, double stepped, and face core center; one at the east face and one at the west face. The beam port heads are 0.426 inches from the core face and are located at the core vertical center. See Figure III. The beam tubes each have two aluminum clad concrete shield plugs, 31 inches long. See Figure IV.

G. Through Tube

The through tube (11) is six inches in diameter and extends from one side of the reactor tank to the other. The minimum distance between the north face of the core and the through tube is 0.378 inches. See Figure III. The center of the through tube is at the same height as the core center. The through tube shield plugs are the same type as those used in the beam ports. See Figure IV.

H. Instrumentation

The reactor power level is monitored and automatically controlled by means of several different channels (12). The startup channel follows the thermal neutron flux build-up from source level to about 0.1 watts. The startup channel system consists of a boron triflouride (BF_3) proportional detector with its associated electronic read-out, control, and power supply equipment. The log N channel provides an indication of neutron level from 0.01 watts to 15 kw. The

log N channel is composed of a compensated ion chamber together with its associated read-out, control, and power supply equipment. The level safety channel supplies and controls magnet current so as to cause a reactor scram, if necessary. The linear level channel supplies a signal linearly proportional to the reactor power level. Consisting of a compensated ion chamber and associated read-out, control, and power supply equipment, the linear level channel operates in eight overlapping ranges, from source level to full power.

SECTION III

PROPERTIES OF THE THRESHOLD NEUTRON DETECTOR FOILS

A. Materials

Sulfur. The sulfur foils are 1/8 inch thick, 1 inch in diameter, and weigh 3 grams each. See Figure V. They are fabricated from flowers of sulfur, 99.89% pure. The particular foils used were purchased from the California Pharmaceutical Laboratory, San Jose, California.

The sulfur isotopes are present in their naturally occurring isotopic ratio as indicated in Table II (13).

TABLE II

Naturally Occurring Sulfur Isotopes and Their Abundance

Isotope	Abundance
S^{32}	95.018%
S^{33}	0.750%
S^{34}	4.215%
S^{36}	0.017%

Products of sulfur, neutron reactions and pertinent isotope data are tabulated in Table III (14).

TABLE III

Products of Sulfur, Neutron Reactions

Product isotope	Reaction	Half-life	Characteristic Emission Beta rays	Gamma rays
P^{32}	$S^{32}(n,p)$	14.3 d	1.7 Mev	
S^{35}	$S^{34}(n,\gamma)$	87.1 d	0.17 Mev	

TABLE III(continued)

Product isotope	Reaction	Half-life	Characteristic Emission	
			Beta rays	Gamma rays
S^{37}	$S^{36}(n,\gamma)$	5.04 m	1.6 Mev	3.1 Mev
P^{33}	$S^{33}(n,p)$	24.4 d	0.25 Mev	
P^{34}	$S^{34}(n,p)$	12.4 s	5.1, 3.2 Mev	2.1, 4.0 Mev
Si^{29}	$S^{32}(n,\alpha)$	stable		
Si^{30}	$S^{33}(n,\alpha)$	stable		
Si^{31}	$S^{34}(n,\alpha)$	2.65 h	1.48 Mev	1.26 Mev
S^{33}	$S^{32}(n,\gamma)$	stable		
S^{34}	$S^{33}(n,\gamma)$	stable		
S^{36}	$S^{35}(n,\gamma)$	stable		
S^{38}	$S^{37}(n,\gamma)$	2.87 h	1.1, 3.0 Mev	1.8 Mev

A cursory glance at Table III shows that a forty-eight hour period between the end of the irradiation and the beginning of counting eliminates all extraneous isotopes except sulfur-35 (S^{35}) and phosphorous-33 (P^{33}). However, both of these isotopes are low energy beta particle emitters, and hence, by electronic discrimination, are easily prevented from influencing the results.

Magnesium. The magnesium foils are about 1/16 inch thick, 1 inch in diameter, and weigh 1 gram each. See Figure V. They are fabricated from the metal, 99.99% pure.

The magnesium isotopes are present in their naturally occurring isotopic ratio as indicated in Table IV (15).

TABLE IV

Naturally Occurring Magnesium Isotopes and Their Abundance

Isotope	Abundance
Mg^{24}	78.7%
Mg^{25}	10.1%
Mg^{26}	11.2%

The products of magnesium, neutron reactions and pertinent isotope data are tabulated in Table V (16).

TABLE V

Products of Magnesium, Neutron Reactions

Product isotope	Reaction	Half-life	Characteristic Emission	
			Beta rays	Gamma rays
Mg^{25}	$Mg^{24}(n,\gamma)$	stable		
Mg^{26}	$Mg^{25}(n,\gamma)$	stable		
Mg^{27}	$Mg^{26}(n,\gamma)$	9.45 m	1.75, 1.59 Mev	0.84, 1.02 Mev
Na^{24}	$Mg^{24}(n,p)$	15.0 h	1.390, 4.17 Mev	1.368, 2.754 Mev
Na^{25}	$Mg^{25}(n,p)$	60 s	4.0, 3.0 Mev	0.39, 0.58, 0.98, 1.60 Mev
Na^{26}	$Mg^{26}(n,p)$	1.04 s	> 5 Mev	
Ne^{21}	$Mg^{24}(n,\alpha)$	stable		
Ne^{22}	$Mg^{25}(n,\alpha)$	stable		
Ne^{23}	$Mg^{26}(n,\alpha)$	40.2 s	4.4, 3.95, 2.4 Mev	0.44, 1.65 Mev
Ne^{24}	$Mg^{27}(n,\alpha)$	3.38 m	1.98, 1.10 Mev	0.47, 0.88 Mev
Mg^{28}	$Mg^{27}(n,\gamma)$	21.4 h	0.459 Mev	0.032, 0.4, 0.95 Mev

Examination of Table V shows that a two hour delay in counting eliminates all resulting products except sodium-24

(Na^{24}) and magnesium-28 (Mg^{28}). Mg^{28} is virtually nonexistant and proper amplifier discriminator adjustment prevents any that may be present from influencing the results.

Aluminum. The aluminum foils are about 1/32 inch thick, 1 inch in diameter, and weigh 1 gram each. See Figure V. They are fabricated from the metal, 99.99% pure.

Aluminum has only one natural isotope, aluminum-27 (Al^{27}). The products of aluminum, neutron reactions and pertinent isotope data are tabulated in Table VI (17).

TABLE VI

Products of Aluminum, Neutron Reactions

Product isotope	Reaction	Half-life	Characteristic Emission	
			Beta rays	Gamma rays
Na^{24}	$Al^{27}(n,\alpha)$	15.0 h	1.39, 4.17 Mev	1.368, 2.754 Mev
Al^{28}	$Al^{27}(n,\gamma)$	2.3 m	2.87 Mev	1.78 Mev
Al^{29}	$Al^{28}(n,\gamma)$	6.6 m	2.5, 1.4 Mev	1.28, 2.43 Mev
Al^{30}	$Al^{29}(n,\gamma)$	3.3 s	5.0 Mev	2.26, 3.52 Mev
Mg^{27}	$Al^{27}(n,p)$	9.45 m	1.75, 1.59 Mev	0.84, 1.02 Mev

A two hour delay time before counting permits the decay of all products except sodium-24 (Na^{24}). Interference from any magnesium-27 (Mg^{27}) is precluded by the proper amplifier discriminator setting. Contributions from isotopes formed by two consecutive neutron absorption are considered in Appendix A.

B. Activation Equations

Assume an isotope A which absorbs neutrons, forming

isotope B.

The variation in concentration of B with time, if A is stable and B is not, is given in equation [1] (18).

$$dB/dt = -\lambda_B B - \sigma_B \phi B + \Sigma_A \phi \qquad [1]$$

At equilibrium

$$dB/dt = 0$$

therefore

$$B_o = \Sigma_A \phi/(\lambda_B + \sigma_B \phi) = \Sigma_A \phi/\lambda_B^* \qquad [2]$$

where

λ_B = decay constant for B

$\lambda_B^* = \lambda_B + \sigma_B \phi$ = effective removal constant for B

B = concentration of isotope B at any time T

B_o = equilibrium concentration of isotope B

Σ_A = macroscopic cross section of parent of isotope B

ϕ = neutron flux

σ_B = microscopic cross section for neutron capture by isotope B

then

$$B(T) = \{\Sigma_A \phi/\lambda_B^*\}\{1 - (\exp -\lambda_B^* T)\}$$

$$= B_o\{1 - (\exp -\lambda_B^* T)\} \qquad [3]$$

After removal fo the foil from the reactor, B continues to decay. Having been out of the reactor for time t, the concentration of B will vary as shown in equation [4].

$$B(t) = B(T)\ (\exp -\lambda_B t)$$

$$= B_o\{1 - (\exp -\lambda_B^* T)\}(\exp -\lambda_B t) \qquad [4]$$

Thus, the activity due to the decay of B is as shown in

equation [5].

$$B(t)\lambda_B = B_o\lambda_B(1 - [\exp \lambda_B^* T][\exp -\lambda_B t]$$
$$= \{\Sigma_A\phi\lambda_B/(\lambda_B + \sigma_B\phi)\}\{1 - [\exp (\lambda_B + \sigma_B\phi)T]\}$$
$$\{\exp -\lambda_B t\} \qquad [5]$$

The values of the parameters for the isotopes under consideration are listed in Table VII (19).

TABLE VII

Parameters for the Detector Isotopes

Isotope	Reaction	Microscopic cross section	Threshold energy	Decay constant
S^{32}	$S^{32}(n,p)P^{32}$	$0.30\times10^{-24}cm^2$	3.0 Mev	0.04846 d^{-1}
Mg^{24}	$Mg^{24}(n,p)Na^{24}$	$0.114\times10^{-24}cm^2$	6.3 Mev	0.0462 h^{-1}
Al^{27}	$Al^{27}(n,\alpha)Na^{24}$	$0.183\times10^{-24}cm^2$	8.1 Mev	0.0462 h^{-1}

Since $\sigma\phi$ and λ are approximately of the same order of magnitude, an iterative process would be required to determine ϕ analytically, if all other data were known. A graphical approach could also be used. For a long term effort, an electronic computer program would be the most economical approach. Another alternative for the determination of ϕ is detailed in Section VI.

SECTION IV

EXPERIMENTAL PROCEDURE FOR FOIL IRRADIATION

A. General

The four reactor regions involved in the study were the west beam port, the through tube, the "glory holes," and the core.

B. West Beam Port

A foil holder was designed to support foils on the central axis of the beam port with a longitudinal separation of five inches and at the walls with a longitudinal separation of ten inches. See Figure VI. Neutron dose at each position was measured with a sulfur, an aluminum, and a magnesium foil. The low cross section of the materials, when coupled with the foil thickness, made shadowing effects negligible (20). The irradiation time was 21.5 minutes at 9.4 kw.

C. Through Tube

A foil holder like that used in the beam port was used in the through tube but the length was proportionally longer. The foils placed on the central axis of the through tube had a longitudinal separation of five inches. The foils at the walls had a longitudinal separation of twenty inches. The side near the core had the first foil at the zero reference point (far end of the tube), whereas the side away from the core had the first foil ten inches from the zero reference

point. The irradiation time was 61 minutes at 9.9 kw.

D. Fuel Element Positions B-5 and D-5; the "Glory Holes"

The foils used to measure the flux in the "glory holes" and in the regular fuel elements were supported by 1/8 inch thick lucite strips with 1 1/4 inch diameter holes milled in them. See Figure VII. The bottom hole was placed so as to have one inch between the strip end and the hole center. The remaining holes were three inches apart on centers. The foils were retained in the strips by waterproof tape. The sulfur foils were kept dry by encasement in rubber bags. The sulfur, magnesium, and aluminum foils were irradiated at the same time, since the foil thickness and cross section were such as to eliminate the need for concern about shadowing effects (21). The reactor was operated for 15 minutes at a power level of 10 kw.

E. Fuel Element Positions D-4, D-6, and D-7

The three elements were initially measured only with magnesium and aluminum foils. The rubber encased sulfur foils were found to be slightly thicker than the fuel plate spacing would accommodate. The metal foils were irradiated for 15 minutes at a power level of 10 kw. The foils were supported by the lucite strips previously described.

F. Fuel Element Positions

B-2, C-4, C-5, C-6, D-4, D-6, D-7, E-5, E-7, and F-3

These fuel elements had only sulfur foils in them for

this irradiation with the exception of B-2, at the edge of the core. The sulfur foils were made waterproof by heat sealing them in five mil thick polyethylene sheet. Such a procedure permitted the completed foil strip to fit between the fuel plates without difficulty. The foils were irradiated for 30 minutes at 9.9 kw.

G. Fuel Element Positions E-5 and D-6

These elements were measured a second time with control rod shim #2 completely withdrawn. A determination of the effect of the boron-10 in the control rod's poison section on the fast neutron flux in adjacent fuel elements could then be made. The foils were irradiated for 7 minutes at 10 kw.

H. Fuel Element Positions F-4, F-5, F-6, F-7, and F-8

These elements were measured with waterproofed sulfur foils held in 1/8 inch thick lucite strips with waterproof pressure-sensitive tape. The foils were irradiated for 15 minutes at a power level of 10 kw.

The magnesium and aluminum foils were omitted from a majority of fuel elements based on the author's experience at other facilities. He has found that the ratio of flux above one threshold to flux above another at a point is generally constant within the sensitivity of the neutron detection techniques used.

All fluxes reported are normalized to the 10 kw power level and are corrected for startup and shutdown activity. The corrections are discussed in Appendices B and C.

SECTION V

COUNTING SYSTEM DESCRIPTION

A. General

The counting system consisted of an automatic sample changer, shield pig, scintillator, preamplifier, amplifier, high voltage power supply, scaler, timer, and data printout device. See Figure VIII.

The automatic sample changer, Baird Atomic Model 750, had been modified to function with a Hamner Electronics Company Model N 276 scaler and N 803 timer. The scintillators were powered by a Hamner Electronics Company Model N 401 high voltage power supply. Signal was taken from a Dumont 6292 photomultiplier tube, through a Hamner Model N 380 preamplifier to a Hamner Model N 302 amplifier. The amplifier output was fed into the scaler-timer complex. Overall resolution of the system is discussed in Appendix D. The scaler and timer outputs were fed into a Hewlett-Packard Model 560A digital recorder, where five digits of time and five digits of counts were printed out automatically for each sample. In order to maintain constant counter-source geometry, each foil was placed on a special planchet, the planchet was placed in a planchet holder designed to function in the automatic sample changer, and a group of planchet holders were placed in the sample changer mechanism. See Figure IX.

B. Sulfur Foil

The emitted radiation of the sulfur foil is a beta particle due to the reaction $S^{32}(n,p)P^{32} \rightarrow S^{32} + \beta$. The scintillator used was an anthracene crystal, 1/2 inch thick and 2 inches in diameter. The detection surface of the crystal was made light tight by means of an aluminized Mylar cover of area density 2.5 mgm/cm^2. The crystal was mounted on a Dumont 6292 photomultiplier tube. See Figure X.

The foil was positioned 1/2 inch below the scintillator which counted from, effectively, infinite thickness. See Figure XI. The foil support was aluminum and the chamber was lined with 1/16 inch thick polyethylene sheet. The shield pig was 3 inches thick and fabricated of iron.

C. Aluminum and Magnesium Foils

Since both of the foils form Sodium-24 (Na^{24}) by the reaction $Mg^{24}(n,p)Na^{24}$ and $Al^{27}(n,\alpha)Na^{24}$, they were counted in the same way. The scintillator was 1 1/2 inches thick and 2 inches in diameter. It was composed of a single crystal of thallium activated sodium iodide [Na(Tl)] mounted on a Dumont 6292 photomultiplier tube. See Figure IX. A 1/2 inch thick lead shield was interposed between the crystal and the foil. For both of the foils, the amplifier discriminator was set for 1.1 Mev. The same shield pig utilized for the sulfur foils was used for the aluminum and magnesium foils.

SECTION VI

CALIBRATION

A. Sulfur Foil

The sulfur foil counting system was calibrated with sulfur foils irradiated in the Cockcroft-Walton accelerator of the Nuclear Defense Laboratory, Edgewood, Maryland, thus activating them with 14 Mev neutrons. An accurate knowledge of the neutron dose was obtained by means of an associated particle count, using alpha scintillators, from the reaction $D(T,n)\alpha$.

The standard sulfur foils were then counted using the system described in Section V. Amplifier gain was varied in order to obtain a calibration number of about 10^9 neutrons per square centimeter per count per second ($n/cm^2/ct/sec$). A standard source of cesium-137 (Cs^{137}) was then counted and the net count rate noted. The Cs^{137} source became the standard by means of which the amplifier gain was set.

The calibration number was determined by averaging the ratios of the neutron dose received by each sulfur foil to the net count rate noted for that foil. A correction was made for the variation of effective cross section with energy. Both the irradiation time and the counting time were short enough to obviate the need for decay corrections.

B. Magnesium and Aluminum Foils

Both the magnesium foils and the aluminum foils were

irradiated in the same Cockcroft-Walton accelerator as the sulfur foils. The metal foils were then counted using the equipment described in Section V. The discriminator setting necessitated the use of cobalt-60 (Co^{60}) as the reference source. The amplifier gain was determined in a manner similar to that described for sulfur foils. Since the neutron dose was known, the calibration number was determined by averaging the ratios of the dose to the net count rate for each metal foil. A correction for the energy dependence of the cross section was then made. Even though the counting time was short enough to eliminate decay corrections, they were necessitated by the length of the irradiation time.

SECTION VII

DATA REDUCTION

A. Sulfur

The sulfur data was handled in the following manner. The gross count rate was determined about every seven days for four weeks, starting 48 hours after the end of the irradiation. The data were corrected for background and gain shift, thus yielding the net count rate. A plot was made of count rate against time on semi-logarithmic graph paper and a straight line was fitted to the data. The line was then extrapolated back to the irradiation time (T_o), and the count rate at zero time (R_o) was determined. Multiplying R_o by the calibration number for the foil yielded the neutron dose which the foil received. Dividing the dose by the irradiation time yielded the flux at the point of irradiation. Generally, irradiation times were so short relative to half-life that decay corrections were unnecessary since the error thus introduced was well within the overall system error.

B. Magnesium and Aluminum

Essentially the same method, as was used for sulfur foils, was utilized for aluminum and magnesium, with the applicable calibration numbers being used to obtain the neutron doses. The counting time was initiated 2 hours after the end of the irradiation, and due to the half-life of

sodium-24 (Na^{24}), the foils were counted morning and evening for four days. There were no variations in the above described technique unless the irradiation time was long relative to the Na^{24} half-life. In such a case, correction for decay during irradiation had to be made.

C. Statistical Limitations

Counting time for all foils was arbitrarily limited to 10,000 counts or 1,000 seconds, whichever occurred first. This assured good counting statistics within reasonable counting times. The need for making corrections for decay during the counting period was eliminated in this manner. The only exception to this rule was in a case when time for 10,000 counts was less than 10 seconds. The total number of counts measured was then increased so that three significant figures were obtained. A sample data point with an error analysis is presented in Appendix E.

The calibration numbers applicable to the detector foils used are listed in Table VIII.

TABLE VIII

Foil Calibration Numbers

Foil	Calibration number, $n/cm^2/ct/sec$	
Sulfur	2.82×10^9	
Magnesium	2.41×10^9	with 1/2 inch thick lead shield
Aluminum	2.17×10^9	with 1/2 inch thick lead shield

SECTION VIII

RESULTS

The neutron flux at all points where detectors were placed is tabulated for easy reference. The flux distribution is plotted, with error flags. See Figures 1 through 25. All errors are ±25%. See Appendix E. The tabulated data is given to two significant figures.

There is a significant difference in the neutron flux distribution and in the peak flux values, since the beam port and through tube have different symmetry conditions. The maximum neutron flux is found at the reactor end of the beam port. The neutron flux at the inner face of the beam port shield plug is about 200 times less than the maximum, for neutrons of energy above 3.0 Mev, 6.3 Mev, and 8.1 Mev, respectively. The maximum neutron flux in the through tube appears at its longitudinal center. The flux decreases at the inner face of the shield plug by factors of about 2,000, 5,000, and 3,000 for neutrons of energy above 3.0 Mev, 6.3 Mev and 8.1 Mev, respectively.

The through tube neutron spectrum shifts considerably from the center to the end, but the beam port spectrum is constant. This is probably due to the placement of the through tube relative to the core. Each point along the length of the through tube sees the reactor through a different tube wall and water shield thickness. Therefore, although the dose received by the through tube is symmetrical

about its longitudinal center, the spectrum varies with length probably due primarily to the moderator thickness variation. The contribution from neutrons scattered into the tube at various angles from the moderator and wall complicate the spectrum, particularly toward the low energy side of the fast neutron region.

The neutron flux above 3.0 Mev in fuel elements D-6 and E-5 with a normal control rod configuration was compared to the neutron flux above 3.0 Mev in fuel elements D-6 and E-5 with a control rod configuration where shim #2 was completely withdrawn. The peak flux decreases from that found with the normal control rod configuration by a factor of 0.61 and 0.66 respectively.

The final fast neutron flux data for the University of Maryland Reactor operating at a power level of 10 kw are tabulated. See Tables IX through XXIX.

TABLE IX

West Beam Port

Distance from reactor end of beam port, in.	Neutron flux, E > 3.0 Mev, n/cm^2-sec	Neutron flux, E > 6.3 Mev, n/cm^2-sec	Neutron flux, E > 8.1 Mev, n/cm^2-sec
Longitudinal axis			
0	2.6×10^9	8.9×10^7	5.2×10^7
5	1.1×10^9	4.5×10^7	2.4×10^7
10	3.7×10^8	1.8×10^7	9.1×10^6
15	1.8×10^8	7.8×10^6	4.1×10^6
20	8.3×10^7	4.7×10^6	2.2×10^6
25	4.8×10^7	2.5×10^6	1.3×10^6
30	3.0×10^7	1.8×10^6	8.7×10^5
35	2.3×10^7	1.5×10^6	5.7×10^5
40	1.6×10^7	9.1×10^5	4.8×10^5
45	1.2×10^7	4.8×10^5	2.7×10^5
Adjacent to north wall			
0	1.7×10^9	6.7×10^7	3.4×10^7
10	2.9×10^8	1.2×10^7	7.0×10^6
20	7.6×10^7	4.3×10^6	1.8×10^6
30	2.8×10^7	1.9×10^6	8.3×10^5
40	1.9×10^7	1.2×10^6	6.0×10^5
Adjacent to south wall			
0	2.4×10^9	8.9×10^7	4.5×10^7
10	2.3×10^8	9.9×10^6	5.7×10^6
20	6.3×10^7	3.3×10^6	1.5×10^6
30	2.6×10^7	1.3×10^6	8.3×10^5
40	1.5×10^7	6.7×10^5	3.4×10^5

TABLE X

Through Tube

Distance from through tube east end, in.	Neutron flux, E > 3.0 Mev, n/cm^2-sec	Neutron flux, E > 6.3 Mev, n/cm^2-sec	Neutron flux, E > 8.1 Mev, n/cm^2-sec
Longitudinal axis			
0	6.7×10^5	2.7×10^4	1.8×10^4
5	1.0×10^6	6.4×10^4	3.9×10^4
10	1.5×10^6	9.0×10^4	5.0×10^4
15	2.4×10^6	1.2×10^5	6.4×10^4
20	3.9×10^6	1.5×10^5	1.2×10^5
25	7.7×10^6	5.0×10^5	2.3×10^5
30	1.8×10^7	1.1×10^6	4.7×10^5
35	4.7×10^7	2.9×10^6	1.7×10^6
40	1.5×10^8	8.0×10^6	5.4×10^6
45	4.8×10^8	1.7×10^7	1.7×10^7
50	1.1×10^9	4.3×10^7	2.4×10^7
55	1.7×10^9	1.0×10^8	5.2×10^7
60	1.6×10^9	6.1×10^7	4.7×10^7
65	8.1×10^8	3.2×10^7	2.3×10^7
70	2.8×10^8	1.4×10^7	1.0×10^7
75	8.7×10^7	5.6×10^6	4.1×10^6
80	3.0×10^7	2.2×10^6	1.4×10^6
85	1.2×10^7	8.6×10^5	5.4×10^5
90	5.5×10^6	3.7×10^5	2.2×10^5
95	3.0×10^6	1.7×10^5	1.3×10^5
100	1.9×10^6	7.6×10^4	5.2×10^4

TABLE X (continued)

Distance from through tube east end, in.	Neutron flux, E > 3.0 Mev, n/cm^2-sec	Neutron flux, E > 6.3 Mev, n/cm^2-sec	Neutron flux E > 8.1 Mev, n/cm^2-sec
105	1.2×10^6	5.3×10^4	3.2×10^4
110	8.0×10^5	2.8×10^4	1.3×10^4
North wall			
10	2.0×10^6	1.1×10^5	3.0×10^4
30	3.1×10^7	2.3×10^6	1.2×10^6
50	1.0×10^9	3.1×10^7	2.6×10^7
70	2.2×10^8	1.1×10^7	6.1×10^6
90	6.7×10^6	7.2×10^5	2.0×10^5
110	9.6×10^5	1.1×10^5	1.5×10^4
South wall			
0	8.2×10^5	1.2×10^5	$< 10^4$
20	3.5×10^6	2.1×10^5	9.1×10^4
40	1.5×10^8	6.0×10^6	2.4×10^6
60	2.0×10^9	8.3×10^7	4.9×10^7
80	1.6×10^7	1.0×10^6	6.5×10^5
100	1.5×10^5	8.6×10^4	2.7×10^4

TABLE XI

Reactor Position B-2 - Outside Core

Height above bottom of fuel element, in.	Neutron flux, E > 3.0 Mev, n/cm^2-sec	Neutron flux, E > 6.3 Mev, n/cm^2-sec	Neutron flux, E > 8.1 Mev, n/cm^2-sec
1	2.7×10^8	4.0×10^7	6.6×10^6
4	3.3×10^8	5.2×10^7	1.0×10^7
7	4.2×10^8	7.4×10^7	1.3×10^7
10	4.7×10^8	7.7×10^7	1.5×10^7
13	4.7×10^8	8.1×10^7	1.4×10^7
16	4.2×10^8	7.2×10^7	1.2×10^7
19	3.2×10^8	5.7×10^7	9.1×10^6
22	2.4×10^8	3.2×10^7	6.6×10^6
25	1.6×10^8	2.0×10^7	4.5×10^6
28	7.6×10^7	7.6×10^6	2.0×10^6

TABLE XII

Outer "Glory Hole" - Fuel Element B-5

Height above bottom of fuel element, in.	Neutron flux, E > 3.0 Mev, n/cm^2-sec	Neutron flux, E > 6.3 Mev, n/cm^2-sec	Neutron flux, E > 8.1 Mev, n/cm^2-sec
1	1.8×10^9	5.8×10^7	3.7×10^7
4	3.7×10^9	9.7×10^7	5.2×10^7
7	5.5×10^9	1.7×10^8	7.8×10^7
10	6.5×10^9	2.0×10^8	1.3×10^8
13	6.9×10^9	2.5×10^8	1.5×10^8
16	6.8×10^9	2.0×10^8	1.1×10^8
19	6.0×10^9	1.6×10^8	8.4×10^7
22	4.1×10^9	1.3×10^8	6.1×10^7
25	1.4×10^9	4.0×10^7	2.7×10^7
28	3.6×10^8	1.7×10^7	8.1×10^6

TABLE XIII

Fuel Element C-4

Height above bottom of fuel element, in.	Neutron flux, E > 3.0 Mev, n/cm^2-sec
1	9.4×10^9
4	1.5×10^{10}
7	1.8×10^{10}
10	1.9×10^{10}
13	1.8×10^{10}
16	1.6×10^{10}
19	1.2×10^{10}
22	4.9×10^9
25	9.4×10^8
28	3.2×10^8

TABLE XIV

Fuel Element C-5

Height above bottom of fuel element, in.	Neutron flux, E > 3.0 Mev, n/cm^2-sec
1	1.0×10^{10}
4	2.1×10^{10}
7	2.6×10^{10}
10	2.8×10^{10}
13	2.9×10^{10}
16	2.4×10^{10}
19	2.0×10^{10}
22	1.5×10^{10}
25	2.8×10^{9}
28	5.3×10^{8}

TABLE XV

Fuel Element C-6

Height above bottom of fuel element, in.	Neutron flux, E > 3.0 Mev, n/cm^2-sec
1	1.1×10^{10}
4	2.0×10^{10}
7	2.8×10^{10}
10	2.9×10^{10}
13	3.0×10^{10}
16	2.6×10^{10}
19	2.3×10^{10}
22	1.4×10^{10}
25	2.4×10^{9}
28	5.4×10^{8}

TABLE XVI

Fuel Element D-4

Height above bottom of fuel element, in.	Neutron flux, E > 3.0 Mev, n/cm^2-sec	Neutron flux, E > 6.3 Mev, n/cm^2-sec	Neutron flux, E > 8.1 Mev, n/cm^2-sec
1	1.4×10^{10}	4.7×10^{8}	1.6×10^{8}
4	2.4×10^{10}	8.7×10^{8}	2.8×10^{8}
7	2.6×10^{10}	1.3×10^{9}	4.0×10^{8}
10	2.9×10^{10}	1.3×10^{9}	4.6×10^{8}
13	3.0×10^{10}	1.3×10^{9}	4.5×10^{8}
16	2.6×10^{10}	1.1×10^{9}	3.6×10^{8}
19	1.8×10^{10}	9.3×10^{8}	2.9×10^{8}
22	8.2×10^{9}	5.3×10^{8}	1.9×10^{8}
25	1.7×10^{9}	1.2×10^{8}	3.7×10^{8}
28	4.6×10^{8}	5.1×10^{7}	1.4×10^{7}

TABLE XVII

Central "Glory Hole" - Fuel Element D-5

Height above bottom of fuel element, in.	Neutron flux, E > 3.0 Mev, n/cm^2-sec	Neutron flux, E > 6.3 Mev, n/cm^2-sec	Neutron flux, E > 8.1 Mev, n/cm^2-sec
1	5.4×10^9	1.9×10^8	1.2×10^8
4	1.3×10^{10}	3.5×10^8	2.9×10^8
7	1.8×10^{10}	4.7×10^8	3.9×10^8
10	2.0×10^{10}	5.9×10^8	4.5×10^8
13	2.0×10^{10}	5.5×10^8	4.2×10^8
16	1.9×10^{10}	4.9×10^8	3.4×10^8
19	1.5×10^{10}	4.7×10^8	3.0×10^8
22	9.7×10^9	2.6×10^8	1.7×10^8
25	3.5×10^9	1.1×10^8	6.8×10^7
28	8.4×10^8	3.0×10^7	1.2×10^7

TABLE XVIII

Fuel Element D-6

Height above bottom of fuel element, in.	Neutron flux, E > 3.0 Mev, n/cm^2-sec	Neutron flux, E > 6.3 Mev, n/cm^2-sec	Neutron flux, E > 8.1 Mev, n/cm^2-sec
1	1.3×10^{10}	4.1×10^{8}	2.0×10^{8}
4	2.7×10^{10}	8.3×10^{8}	3.8×10^{8}
7	3.6×10^{10}	1.2×10^{9}	5.7×10^{8}
10	4.1×10^{10}	1.6×10^{9}	7.6×10^{8}
13	4.2×10^{10}	1.7×10^{9}	7.3×10^{8}
16	3.5×10^{10}	1.1×10^{9}	7.4×10^{8}
19	2.7×10^{10}	9.4×10^{8}	5.4×10^{8}
22	1.6×10^{10}	5.8×10^{8}	3.8×10^{8}
25	3.4×10^{9}	2.0×10^{8}	8.0×10^{7}
28	6.9×10^{8}	1.3×10^{8}	2.1×10^{7}

TABLE XIX

Fuel Element D-7

Height above bottom of fuel element, in.	Neutron flux, E > 3.0 Mev, n/cm^2-sec	Neutron flux, E > 6.3 Mev, n/cm^2-sec	Neutron flux E > 8.1 Mev, n/cm^2-sec
1	1.1×10^{10}	4.1×10^{8}	1.1×10^{8}
4	2.0×10^{10}	7.1×10^{8}	2.5×10^{8}
7	2.7×10^{10}	1.0×10^{9}	3.5×10^{8}
10	3.1×10^{10}	1.2×10^{9}	4.1×10^{8}
13	3.1×10^{10}	1.4×10^{9}	4.2×10^{8}
16	2.6×10^{10}	1.3×10^{9}	4.2×10^{8}
19	2.2×10^{10}	1.1×10^{9}	2.9×10^{8}
22	1.4×10^{10}	6.7×10^{8}	2.1×10^{8}
25	2.6×10^{9}	2.4×10^{8}	4.6×10^{7}
28	5.0×10^{8}	9.1×10^{7}	1.6×10^{7}

TABLE XX

Fuel Element E-5

Height above bottom of fuel element, in.	Neutron flux, E > 3.0 Mev, n/cm^2-sec
1	1.5×10^{10}
4	2.7×10^{10}
7	3.1×10^{10}
10	3.7×10^{10}
13	3.9×10^{10}
16	3.7×10^{10}
19	2.7×10^{10}
22	1.7×10^{10}
25	3.1×10^{9}
28	6.6×10^{8}

TABLE XXI

Fuel Element E-7

Height above bottom of fuel element, in.	Neutron flux, E > 3.0 Mev, n/cm^2-sec
1	8.7×10^9
4	1.7×10^{10}
7	2.5×10^{10}
10	2.9×10^{10}
13	3.5×10^{10}
16	2.7×10^{10}
19	2.3×10^{10}
22	1.4×10^{10}
25	3.3×10^9
28	8.0×10^8

TABLE XXII

Fuel Element F-3

Height above bottom of fuel element, in.	Neutron flux, E > 3.0 Mev, n/cm^2-sec
1	6.9×10^9
4	1.0×10^{10}
7	1.4×10^{10}
10	1.6×10^{10}
13	1.5×10^{10}
16	1.4×10^{10}
19	1.0×10^{10}
22	4.1×10^9
25	6.9×10^8
28	2.4×10^8

TABLE XXIII

Fuel Element F-4

Height above bottom of fuel element, in.	Neutron flux, E > 3.0 Mev, n/cm^2-sec
1	6.9×10^9
4	1.4×10^{10}
7	1.9×10^{10}
10	2.1×10^{10}
13	2.1×10^{10}
16	1.8×10^{10}
19	1.4×10^{10}
22	8.1×10^9
25	1.4×10^9
28	3.2×10^8

TABLE XXIV

Fuel Element F-5

Height above bottom of fuel element, in.	Neutron flux, E > 3.0 Mev, n/cm^2-sec
1	6.0×10^9
4	1.6×10^{10}
7	2.2×10^{10}
10	2.6×10^{10}
13	2.5×10^{10}
16	2.3×10^{10}
19	1.8×10^{10}
22	1.2×10^{10}
25	2.8×10^9
28	5.2×10^8

TABLE XXV

Fuel Element F-6

Height above bottom of fuel element, in.	Neutron flux, E > 3.0 Mev, n/cm^2-sec
1	7.4×10^9
4	1.6×10^{10}
7	2.2×10^{10}
10	2.6×10^{10}
13	2.7×10^{10}
16	2.3×10^{10}
19	1.8×10^{10}
22	1.1×10^{10}
25	2.2×10^9
28	4.7×10^8

TABLE XXVI

Fuel Element F-7

Height above bottom of fuel element, in.	Neutron flux, E > 3.0 Mev, n/cm^2-sec
1	6.2×10^9
4	1.3×10^{10}
7	1.7×10^{10}
10	1.9×10^{10}
13	1.9×10^{10}
16	1.7×10^{10}
19	1.4×10^{10}
22	8.8×10^9
25	1.7×10^9
28	3.6×10^8

TABLE XXVII

Fuel Element F-8

Height above bottom of fuel element, in.	Neutron flux, E > 3.0 Mev, n/cm^2-sec
1	5.7×10^9
4	1.0×10^{10}
7	1.2×10^{10}
10	1.4×10^{10}
13	1.5×10^{10}
16	1.3×10^{10}
19	1.1×10^{10}
22	7.1×10^9
25	1.4×10^9
28	2.9×10^8

TABLE XXVIII

Fuel Element D-6 - Shim #2 Withdrawn

Height above bottom of fuel element, in.	Neutron flux, E > 3.0 Mev, n/cm^2-sec
1	1.2×10^{10}
4	1.9×10^{10}
7	2.5×10^{10}
10	2.6×10^{10}
13	2.5×10^{10}
16	2.3×10^{10}
19	1.7×10^{10}
22	9.4×10^{9}
25	1.3×10^{9}
28	3.0×10^{8}

TABLE XXIX

Fuel Element E-5 - Shim #2 Withdrawn

Height above bottom of fuel element, in.	Neutron flux, E > 3.0 Mev, n/cm^2-sec
1	8.3×10^9
4	1.7×10^{10}
7	2.2×10^{10}
10	2.5×10^{10}
13	2.6×10^{10}
16	2.3×10^{10}
19	1.8×10^{10}
22	1.2×10^{10}
25	2.3×10^9
28	5.0×10^8

SECTION IX

CONCLUSIONS AND FUTURE WORK

A. Conclusions

The design analysis of the University of Maryland Reactor (UMR) gave a maximum fast neutron flux of 8.75×10^{11} n/cm^2-sec (22). This was considered to be above an energy of 0.1 to 1.0 Kev. The maximum fast neutron flux above 3.0 Mev observed by the author was $4.2 \times 10^{10} n/cm^2$-sec in a fully loaded fuel element position. The spectral distribution of a General Atomic TRIGA reactor, which should be similar to that of the UMR, has a ratio of neutrons with energy above 1.0 Kev to those with energy above 3.0 Mev of about 20 (23). Using this ratio, the neutron flux above 1.0 Kev at the UMR is $8.4 \times 10^{11} n/cm$ -sec.

The maximum fast neutron flux in the central and outer "glory holes" was measured for neutrons of energy above 3.0 Mev, 6.3 Mev, and 8.1 Mev. Above 3.0 Mev, the fluxes are about $2.0 \times 10^{10} n/cm^2$-sec and $6.9 \times 10^{9} n/cm^2$-sec, respectively. Above 6.3 Mev, the fluxes are about $5.9 \times 10^{8} n/cm^2$-sec and $2.4 \times 10^{8} n/cm^2$-sec, respectively. Above 8.1 Mev, the fluxes are, respectively, $4.5 \times 10^{8} n/cm^2$-sec and $1.5 \times 10^{8} n/cm^2$-sec.

At the reactor end of the west beam port, the maximum neutron fluxes are about $2.6 \times 10^{9} n/cm^2$-sec, $8.9 \times 10^{7} n/cm^2$-sec, and $5.2 \times 10^{7} n/cm^2$-sec above the energies of 3.0 Mev, 6.3 Mev, and 8.1 Mev, respectively. The minimum fluxes at the inside of the beam port shield plugs are, respectively, 1.2×10^{7}

n/cm^2-sec, $4.8 \times 10^5 n/cm^2$-sec, and $2.7 \times 10^5 n/cm^2$-sec.

The maximum central fast neutron flux and its variation from wall to wall in the through tube was measured for neutrons with energy above 3.0 Mev, 6.3 Mev, and 8.1 Mev. The neutron flux with energy greater than 3.0 Mev is 1.7×10^9 n/cm^2-sec on the axis and varies across the diameter from about 3.0 to $1.0 \times 10^9 n/cm^2$-sec. The neutron flux with energy greater than 6.3 Mev is $1.0 \times 10^8 n/cm^2$-sec and varies across the diameter from 1.2×10^8 to $5.0 \times 10^7 n/cm^2$-sec. For energy greater than 8.1 Mev the neutron flux is $5.2 \times 10^7 n/cm^2$-sec and varies across the diameter from about 6.0 to 3.5×10^7 n/cm^2-sec.

Above 3.0 Mev, the fast neutron flux in fuel element positions E-5 and D-6 is lower with control rod shim #2 fully withdrawn than with the rod partially inserted.

About 1 1/2 inches above the fuel containers of the core and, therefore, in the water reflector, the flux above 3.0 Mev has a maximum of $8.4 \times 10^8 n/cm^2$-sec and a minimum of $2.4 \times 10^8 n/cm^2$-sec.

The vertical fast neutron flux distribution curves show a modified cosine distribution. See Figures 1 through 19.

The vertical fast neutron flux distribution at the side of the core (position B-2) is asymmetric; a condition which may be the result of partial removal of the control rods. The peak fission rate and, hence, the fast neutron flux are displaced below the vertical center of the core.

The central "glory hole" (position D-5) is a water channel with thermal neutron flux peaking. The peaking effect would tend to cause the vertical neutron flux distribution to be symmetrical about the vertical center of the core. The distribution is symmetrical for fast neutrons. See Figure 7.

The remaining fuel elements exhibit peak neutron flux displacement below the core vertical center. This is presumed to relate to the partially withdrawn control rods. The effect is clearly seen for neutrons of energy greater than 3.0 Mev. For neutrons above the higher thresholds, no displacement is noted in fuel elements D-6 and D-7, while displacement is noted in fuel element D-4. The cause may be the presence of the central "glory hole" adjacent to position D-6 and of the water-filled, stainless steel regulating rod adjacent to position D-7. Therefore, there is a water channel in which thermal flux peaking may occur adjacent to each position.

B. Future Work

The development of a system of threshold or other type of detectors to provide fast neutron dosimetry in high intensity, mixed radiation fields is the present long term goal of the author. Although fission reactions can be utilized down to energies as low as 1.5 Kev, there are very large gaps above that energy with no available material for detection.

The most promising approach to the goal now appears to be the utilization of the n,n' reaction, or, as it is sometimes called, isomeric state formation. Half-lives of the states are conveniently short, the materials are usually stable, and, in many cases, the naturally occurring isotopic mixtures may be used.

The great disadvantages lie in the dearth of knowledge of n,n' reaction cross sections and in the difficulty of having investigations performed to determine the reaction cross sections in the energy range of interest.

The fruition of the goal will enable any interested group to carry out its own fast neutron dosimetry program if it has a general license for irradiated material. No longer will procurement of an Atomic Energy Commission license to purchase the detector materials themselves be necessary. The insertion of the materials into a reactor system will be much less hazardous since large thermal neutron sinks of boron-10 will not be needed as thermal neutron shields.

APPENDIX A

ACTIVITY CONTRIBUTIONS FROM ISOTOPES FORMED BY TWO CONSECUTIVE NEUTRON ABSORPTIONS

The probability of an isotope α absorbing a neutron and forming isotope β and β , in turn, absorbing a neutron and forming isotope γ is, in general, small. However, one must be cognizant of the possibility at all times. See Tables A-I and A-II for the sulfur and magnesium foil reactions.

There is no table for the aluminum foil since aluminum-27 (Al^{27}) is 100% abundant. See Section III in the body of the paper for analysis. Note that magnesium-27 (Mg^{27}) is produced. See Table A-II for the reaction products.

In all cases, either the half-life is extremely short or the radiation energy is below that of the discriminator setting. The only isotope not eliminated by either condition is magnesium-28 (Mg^{28}), with a half-life of 21.4 hours and a gamma ray with energy of 1.35 Mev.

The cross section of Mg^{27} for the production of Mg^{28} is not, at present, available. Considering its parent, the macroscopic cross section of Mg^{28} is probably small (A-1). The cross section of Mg^{26} is also small (A-2). Thus, the quantity of Mg^{28} formed contributes a very small part to the overall count rate of the sodium-24 (Na^{24}). Any contribution from Mg^{28} is well within experimental error for this type of detector. For most of the points at which data was taken, any contributing activity is below the background count rate.

TABLE A-I

Products of Multiple Neutron Absorption by Sulfur

Stable parent, α	First product, β	Half-life, β	Second product, γ	Half-life, γ	Abundance of α	Cross section of β	Beta, Mev	Gamma, Mev
S^{32}	P^{32}	14.3 d	P^{33}	24.4 d	95.018%	N/A	0.248	
	Si^{29}	stable	Si^{30}	stable	95.018%	0.27 barns		
	S^{33}	stable	S^{34}	stable	95.018%	0.0023 barns		
S^{33}	P^{33}	24.4 d	P^{34}	12.4 s	0.750%	N/A	5.1, 3.2	2.1, 4.0
	Si^{30}	stable	S^{31}	2.65 h	0.750%	0.11 barns	1.476	1.26
	S^{34}	stable	S^{35}	87.1 d	0.750%	0.26 barns	0.167	
S^{34}	S^{35}	87.1 d	S^{36}	stable	4.215%	N/A		
	P^{34}	12.4 s	no existence of P^{35} shown					
	Si^{31}	2.65 h	Si^{32}	$7x10^2$ y	4.215%	N/A	0.1	
S^{36}	S^{37}	5.04 m	S^{38}	2.87 h	0.017%	N/A	1.1, 3.0	1.88

TABLE A-II

Products of Multiple Neutron Absorption by Magnesium

Stable parent α	First product, β	Half-life, β	Second product, γ	Half-life, γ	Abundance of α	Cross section of β	Beta, Mev	Gamma, Mev
Mg^{24}	Mg^{25}	stable	Mg^{26}	stable	78.7%	0.27 barns		
	Na^{24}	15.0 h	Na^{25}	60 s	78.7%	N/A	1.39, 4.17	1.368, 4.0 2.754, 5.3
	Ne^{21}	stable	Ne^{22}	stable	78.7%	N/A		
Mg^{25}	Mg^{26}	stable	see below		10.11%	0.027 barns		
	Na^{25}	60 s	Na^{26}	1.04 s	10.11%	N/A	> 5.0	
	Ne^{22}	stable	Ne^{23}	40.2 s	10.11%	N/A	4.4, 3.95 2.4	.44, 1.65
Mg^{26}	Mg^{27}	9.45 m	Mg^{28}	21.4 h	11.29%	N/A	.459	.0032, 0.4, .95, 1.35
	Mg^{27}	9.45 m	Ne^{24}	3.38 m	11.29%	N/A	1.98, 1.10	0.47, 0.88
	Na^{26}	1.04 s	Na^{27}	no existence shown				
	Ne^{23}	40.2 s	Ne^{24}	see above		N/A	1.98, 1.10	0.472, 0.88

APPENDIX B

INDUCED ACTIVITY DURING REACTOR STARTUP

A typical plot of reactor power at startup is shown.

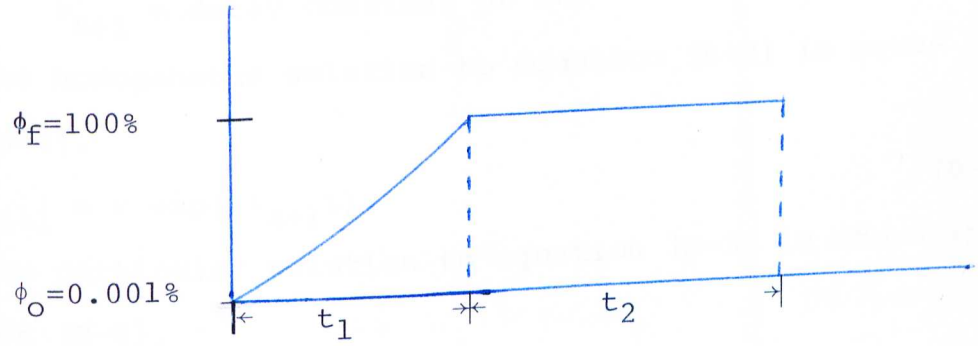

During the time interval t_1, the neutron flux will vary with time as shown in equation [B-1] (B-1).

$$\phi = \phi_o \exp(\xi t) \qquad [B\text{-}1]$$

where

ϕ = neutron flux at any time, t

ϕ_f = neutron flux at steady state power

ϕ_o = neutron flux at some arbitrary low power level, usually 0.001% ϕ_f

ξ = the exponential factor, which is related to the reactor period

For a time interval t the expression for ξ becomes equation [B-2].

$$\xi = (\ell n\{\phi/\phi_o\})/t \qquad [B\text{-}2]$$

The rate of isotope formation is expressed in the manner shown in equation [B-3] (B-2).

$$dN_A/dt = \sigma_A N_A \phi_o \exp(\xi t) - N_{A+1}\lambda_{A+1} \qquad [B\text{-}3]$$

where

σ_A = microscopic cross section of isotope A

N_A = number of atoms of A being irradiated

N_{A+1} = number of atoms of A+1 formed

λ_{A+1} = decay constant of A+1

The homogeneous solution to equation [B-3] is equation [B-4].

$$N_{A+1} = \kappa \exp(-\lambda_{A+1} t) \qquad [B-4]$$

The particular solution to equation [B-3] is shown in equation [B-5].

$$N_{A+1} = \sigma_A N_A \phi_o \exp\{\xi t/(\lambda_{A+1}+\xi)\} \qquad [B-5]$$

The general solution to equation [B-3] is shown in equation [B-6].

$$N_{A+1} = \kappa \exp(-\lambda_{A+1} t) + \sigma_A N_A \phi_o \exp\{\xi t/(\lambda_{A+1} + \xi)\} \qquad [B-6]$$

A value for κ must be obtained. Assume that t equals 0.

$$N_{A+1} = 0 = \kappa + \sigma_A N_A \phi_o/(\lambda_{A+1} + \xi) \qquad [B-7]$$

$$\kappa = -\sigma_A N_A \phi_o/(\lambda_{A+1} + \xi) \qquad [B-8]$$

therefore

$$N_{A+1} = [\sigma_A N_A \phi_o/(\lambda_{A+1} + \xi)][\exp \xi t - \exp(-\lambda_{A+1} t)] \qquad [B-9]$$

The quantity of a particular isotope formed during startup and approach to power may be calculated from equation [B-9]. The foil activity can be corrected for this quantity. A sample calculation will determine the magnitude of the correction required. The following values are assumed in order to facilitate the computation.

$\phi_f = 5 \times 10^{10} n/cm^2\text{-sec}$

$\phi_o = 5 \times 10^{5}\ n/cm^2\text{-sec}$

$\lambda = 5.6 \times 10^{-7} sec^{-1}$

$\Sigma = N\sigma = \rho N_a \sigma / A = 0.0113\ cm^{-1}$

$t = 0.25$ hours

From equation [B-2] we can calculate ξ.

$\xi = 1.28 \times 10^{-2} sec^{-1}$

therefore

$N_{A+1} = 4.4 \times 10^{10} particles/cm^3$

Each foil has a volume of about 1.62 cm^3. Therefore, the number of active particles produced in each foil is about 7×10^{10}. For a material such as phosphorous-32 the decay rate is 4×10^{4} disintegrations per second. Since the source under consideration is in a sulfur matrix with a thickness of 0.3 cm and a density of about 2 g/cm^3, only a fraction of the total number of emitted beta particles will escape from the matrix. Only about 30% of all beta particles which leave the source actually enter the detector. The overall efficiency of the detector-source system is estimated by the author to be 10^{-2}. The activation due to startup will produce a dose equivalent of $1.13 \times 10^{12} n/cm^2$. This is about 10% of the measured total dose. For shorter reactor operating times, the percentage of dose due to startup would increase. Even under the best conditions, a significant contribution due to activation prior to attainment of steady state conditions, would result. Correction for this activity has been made in the final results.

APPENDIX C

INDUCED FOIL ACTIVITY DUE TO THE TIME VARYING NEUTRON FLUX AFTER REACTOR SHUTDOWN

An equation must be developed for determining the number of active nucleii which are present in a foil as a result of the time varying neutron flux during reactor shutdown.

Three conditions must be assumed.

1. A step insertion of all control rods in less than one second.
2. The reactor has been operating for X minutes with a neutron flux of ϕ_o n/cm^2-sec
3. The fast neutron flux decay with time follows the thermal neutron flux.

The variation of flux with time is given by equation [C-1] (C-1).

$$\phi = \phi_o [\beta/(\beta-\rho) \exp(\lambda\rho t/\{\beta-\rho\} - \rho/\{\beta-\rho\} \exp(-\{\beta-\rho\}t/\ell] \quad [C-1]$$

where

ϕ_o = initial neutron flux

β = delayed neutron fraction

ρ = reactivity addition

λ = average one group delayed neutron fraction decay constant

ℓ = prompt neutron lifetime

The formation rate of radioactive material is given by equation [C-2] when the half-life is long relative to the

irradiation time (C-2).

$$dN_{A+1}/dt = N_A\sigma_A\phi(t) \qquad [C\text{-}2]$$

Combining equations [C-1] and [C-2] yields the formation rate of N_{A+1} when N_A is irradiated in a time varying neutron flux.

$$dN_{A+1}/dt = N_A\sigma_A\phi_o[\beta/\{\beta-\rho\}\exp(\lambda\rho t/\{\beta-\rho\} - \rho/\{\beta-\rho\}\exp(-\{\beta-\rho\}t/\ell] \qquad [C\text{-}3]$$

Solving equation [C-3] for N_{A+1}, the number of radioactive nucleii formed is shown in equation [C-4].

$$N_{A+1} = N_A\sigma_A\phi_o[\beta/\lambda\rho\ \exp(\lambda\rho t/\{\beta-\rho\} - \ell\rho/\{\beta-\rho\}^2\exp(-\{\beta-\rho\}t/\ell \Big|_{t=0}^{T} \qquad [C\text{-}4]$$

A sample calculation will determine whether or not significant activity is induced in the detector foils during the decay of the neutron population after reactor scram. The constants for the University of Maryland Reactor are listed below (C-3).

$\rho = 5.27\text{x}10^{-2}$

$\beta = 0.0073$

$\lambda = 0.08\ \text{sec}^{-1}$

$\ell = 7.2\text{x}10^{-5}\text{sec}$

$\phi_o = 5\text{x}10^{10}\text{n/cm}^2\text{-sec}$

$T = 3.6\text{x}10\ \text{sec}$

$N_A\sigma_A = 1.13\text{x}10^{-2}\text{cm}^{-1}$ for sulfur

Now equation [C-4] can be evaluated.

$N_{A+1} = 9.72\text{x}10^{9}$ activated nucleii

The decay rate is given by equation [C-5].

[C-5]

$$dN_{A+1}/dt = N_{A+1}\lambda$$
$$= 5.44 \times 10^{3} \text{ dis/sec}$$

The efficiency of detection, considering source, emitted particle, and geometry, from Appendix B, is about 10^{-2}. The activation then yields about 55 counts per second to initial count rate of the foil. However, the development of equation [C-1] assumes small reactivity changes, and one group of delayed neutrons. Hence, the actual activity due to neutrons produced in this way is probably larger by a factor of 5. Correction for the activity is necessary.

APPENDIX D

RESOLUTION OF THE COUNTING SYSTEM

The counting system specifications are such that resolution and coincidence losses at the count rates experienced in this work are negligible. The photomultiplier-scintillator assemblies have a resolution equivalent to 10^7 pulses per second. All the electronic equipment has linear response rates that are no lower than 10^6 pulses per second. Therefore, the highest count rate foil measured, that of about 5,000 counts per second, is still three orders of magnitude below the limits of the equipment used.

APPENDIX E

REPRESENTATIVE CALCULATION OF A DATA POINT

The raw data from sulfur foil #737 is used for a representative data point calculation. See Table E-I. The reactor power history pertaining to that foil is also given. See Table E-II. The zero time for the foil irradiation, T_o, is May 13, 1965.

A correction factor for startup and shutdown activity, combined with a conversion factor from total dose to flux, is developed. All error estimates of power level and time determination were made by either the author or the reactor operator.

$$\phi_P = D_T[E_P/E_T][1/T_P] \qquad [E\text{-}1]$$

where

ϕ_P = flux at a power level of 10 kw

D_T = total neutron dose measured

E_P = total energy generated by reactor at a power level of 10 kw

E_T = total energy generated during operation

T_P = time at 10 kw

The following information is calculated from the reactor power history.

$$E_P/E_T = 0.67 \qquad [E\text{-}2]$$

The error in equation [E-2] is given in equation [E-3].

$$E_R = 0.67\sqrt{(0.09/300)^2+(0.18/448.5)^2}$$
$$= 3.35\times10^{-4} \qquad [E\text{-}3]$$

The error in the time measurement E_t is estimated to be about 1.6×10^{-6}. The variables in equation [E-1] are replaced by the numerical values appropriate to sulfur foil #737, yielding equation [E-4].

$$\phi_P = D_T(3.7 \times 10^{-4} \pm 1.1 \times 10^{-6}) = D_T(3.7 \times 10^{-4} \pm 0.3\%) \quad [E-4]$$

The count rate at T_o was determined to be $9,850 \pm 3\%$ counts per second. See Figure 26. The calibration number for this foil is $2.82 \times 10^9 n/cm^2/ct/sec \pm 25\%$. See Table VIII.

$$D_T = (9,850 \pm 296)(2.82 \pm 0.70)(10^9) = 2.78 \pm 0.70 \times 10^{13} n/cm^2 = 2.78 \times 10^{13} \pm 25\% n/cm^2 \quad [E-5]$$

The dose yielded by equation [E-5] is then used in equation [E-4] to obtain the neutron flux at a power level of 10 kw.

$$\phi_P = (2.78 \pm 0.70)10^{13}(3.7 \pm 0.011)10^{-4} = 1.03 \times 10^{10} \pm 25\% \quad [E-6]$$

TABLE E-I

Raw Data of Sulfur Foil #737

Date 1965	Counts	Standard deviation	Time sec	Bkgd counts	Standard deviation	Gross counts	Standard deviation	Net count rate, counts/sec
5/17	10^5	316	12.2	6.1	2.5	99,993.9	316.2	8,196.2±25.9≡8,196.2±0.32%
5/27	10^5	316	19.4	11.6	3.4	99,988.4	316.2	5,154.0±16.3≡5,154.0±0.32%
6/7	$5x10^4$	224	16.0	11.2	3.3	49,988.8	223.6	3,124.3±11.0≡3,124.3±0.45%
6/15	$5x10^4$	224	23.5	14.1	3.8	49,985.9	223.6	2,127.1± 9.5≡2,127.1±0.45%

TABLE E-II

Reactor Power History

Time	Power level
10:55	0.1 watts ± 0.1%, 0.1 ± 10^{-4} watts
11:07	10 kw ± 0.1%, 10 kw ± 10 watts
11:37	scram

Positive period - 50 seconds

Total energy generated to reach 10 kw = 59.4 kw-min±.05%

Total energy generated at 10 kw = 300 kw-min±.03%

Total energy generated during decay to 0.1 watts after scram = 89.1 kw-min±.05%

Total energy generated for the complete irradiation was 448.5 kw-min±.04%.

APPENDIX F

POWER GENERATION DUE TO FAST FISSION

The equation for the virgin fast neutron flux is given in equation [F-1](F-1).

$$\phi_v = K\nu P_s/\Sigma \qquad [F\text{-}1]$$

where

ϕ_v = virgin fast neutron flux

K = number of fissions per watt

ν = number of neutrons per fission

P_s = specific power, watts/cm^3

Σ = total macroscopic cross section for virgin neutrons

For the University of Maryland Reactor (UMR) the following values probably apply.

ν = 2.47 (F-2)

K = 3.12×10^{10} fissions/watt (F-3)

Σ = 0.058 (F-4)

The value for Σ is very difficult to determine and the error in the assumed value could be very large.

Replacing the variables with numerical values and rearranging equation [F-1], the specific power as a function of virgin neutron flux is obtained as shown in equation [F-2].

$$P_s = 6.5 \times 10^{-13} \phi_v \qquad [F\text{-}2]$$

Assuming an average flux based on a cosine distribution, the average specific power generated in each fuel element may be computed. See Table F-I. However, fuel elements

C-7, E-4 and E-6 have no flux value assigned since they were inaccessible for data acquisition. The average fluxes are so well grouped in the measured elements that the assumption of a fast neutron flux of 10^{10}n/cm^2-sec would seem reasonable.

Using equation [E-2], the average power generated per cubic centimeter of fuel per element may be calculated. The results are shown in Table F-I.

The total power generated in each fuel element is then computed as the product of the specific power and the volume of fissionable material in the element. Summing the power generated in each element in the UMR, the total power generated by fissioning of nucleii through absorption of neutrons whose energy is greater than 3.0 Mev when the reactor is at a power level of 10 kw is obtained. The total power generated is 2.16 watts.

The low figure is expected for a number of reasons. The neutron fluxes under consideration are small. The reactor fuel is fully enriched(93.5% - U^{235}) and hence there is relatively little U^{238} for the production of a large fast fission effect. An insignificant quantity of power is generated from fissioning caused by neutrons with energy above 3.0 Mev.

TABLE F-I

Fast Neutron Power Generation

in the University of Maryland Reactor

Fuel element	Average flux, n/cm^2-sec	Average power, watts/cm^3/element	Fuel volume, cm^3/element	Total power per element, watts
B-5	4.9×10^9	2.9×10^{-3}	3.85	0.01
C-4	1.3×10^{10}	8.5×10^{-3}	7.7	0.07
C-5	1.8×10^{10}	1.2×10^{-2}	8.56	0.10
C-6	2.0×10^{10}	1.3×10^{-2}	8.56	0.11
C-7	1.0×10^{10}	6.5×10^{-3}	5.14	0.03
D-4	2.0×10^{10}	1.3×10^{-2}	8.56	0.11
D-5	1.3×10^{10}	8.5×10^{-3}	4.82	0.04
D-6	2.6×10^{10}	1.7×10^{-2}	8.56	0.15
D-7	2.1×10^{10}	1.4×10^{-2}	8.56	0.12
E-4	1.0×10^{10}	6.5×10^{-3}	5.14	0.34
E-5	2.6×10^{10}	1.7×10^{-2}	8.56	0.15
E-6	1.0×10^{10}	6.5×10^{-3}	5.14	0.34
E-7	2.1×10^{10}	1.4×10^{-2}	8.56	0.12
F-3	9.9×10^9	6.4×10^{-3}	8.56	0.06
F-4	1.4×10^{10}	9.1×10^{-3}	8.56	0.08
F-5	1.7×10^{10}	1.1×10^{-2}	8.56	0.10
F-6	1.7×10^{10}	1.1×10^{-2}	8.56	0.10
F-7	1.3×10^{10}	8.5×10^{-3}	8.56	0.07
F-8	9.6×10^9	6.2×10^{-3}	9.63	0.06

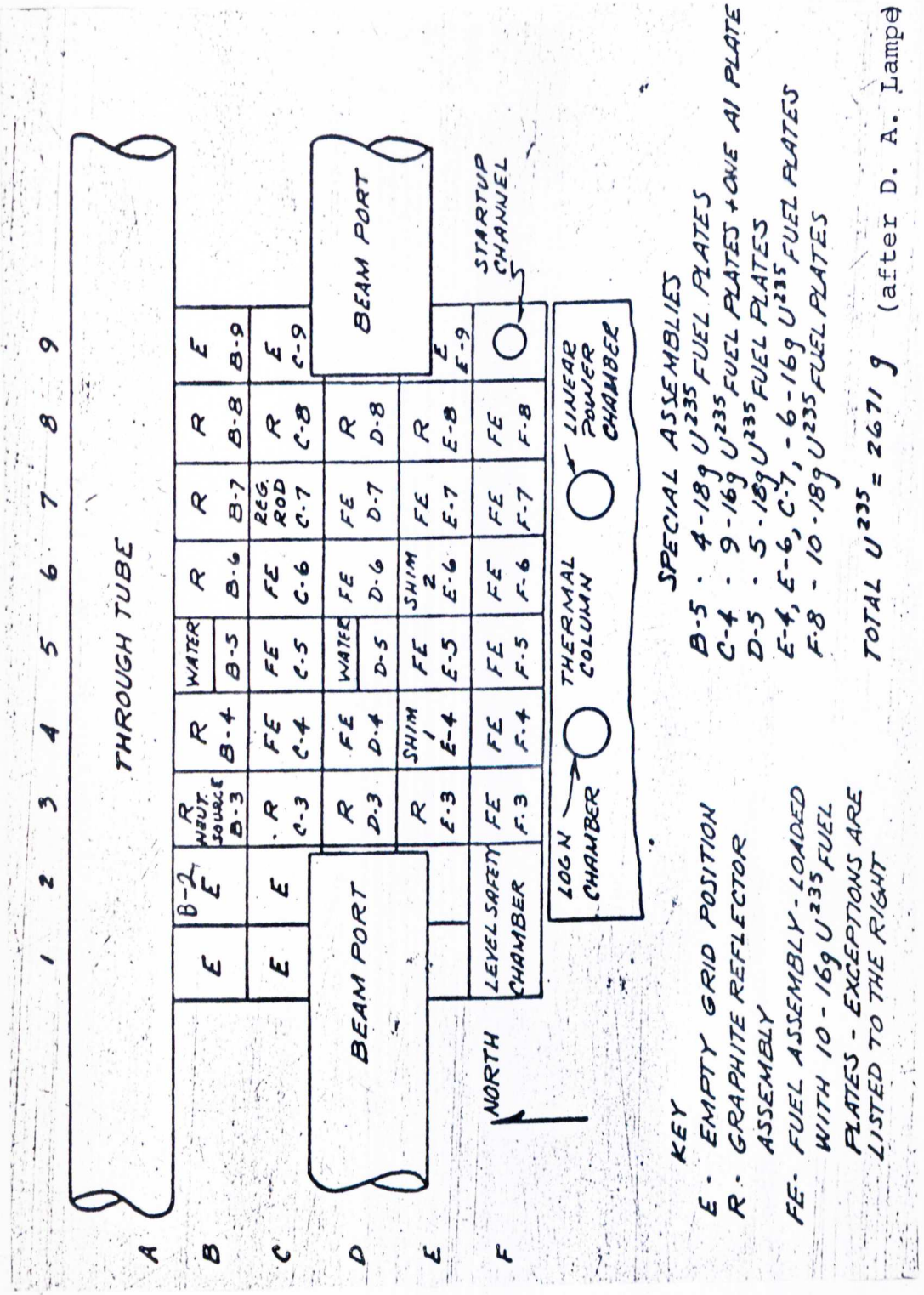

FIGURE I

UNIVERSITY OF MARYLAND

REACTOR CORE PLAN

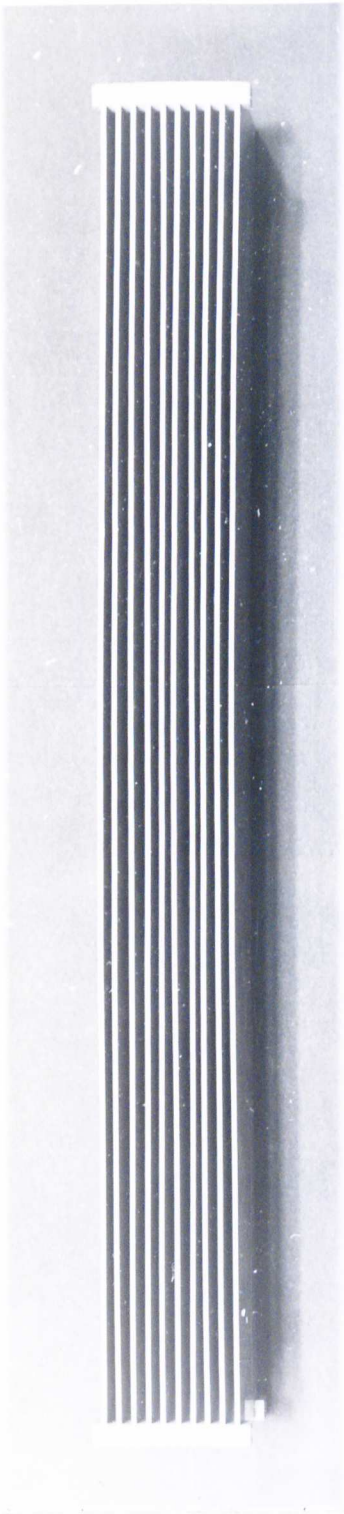

FIGURE II

FUEL PLATE ASSEMBLY

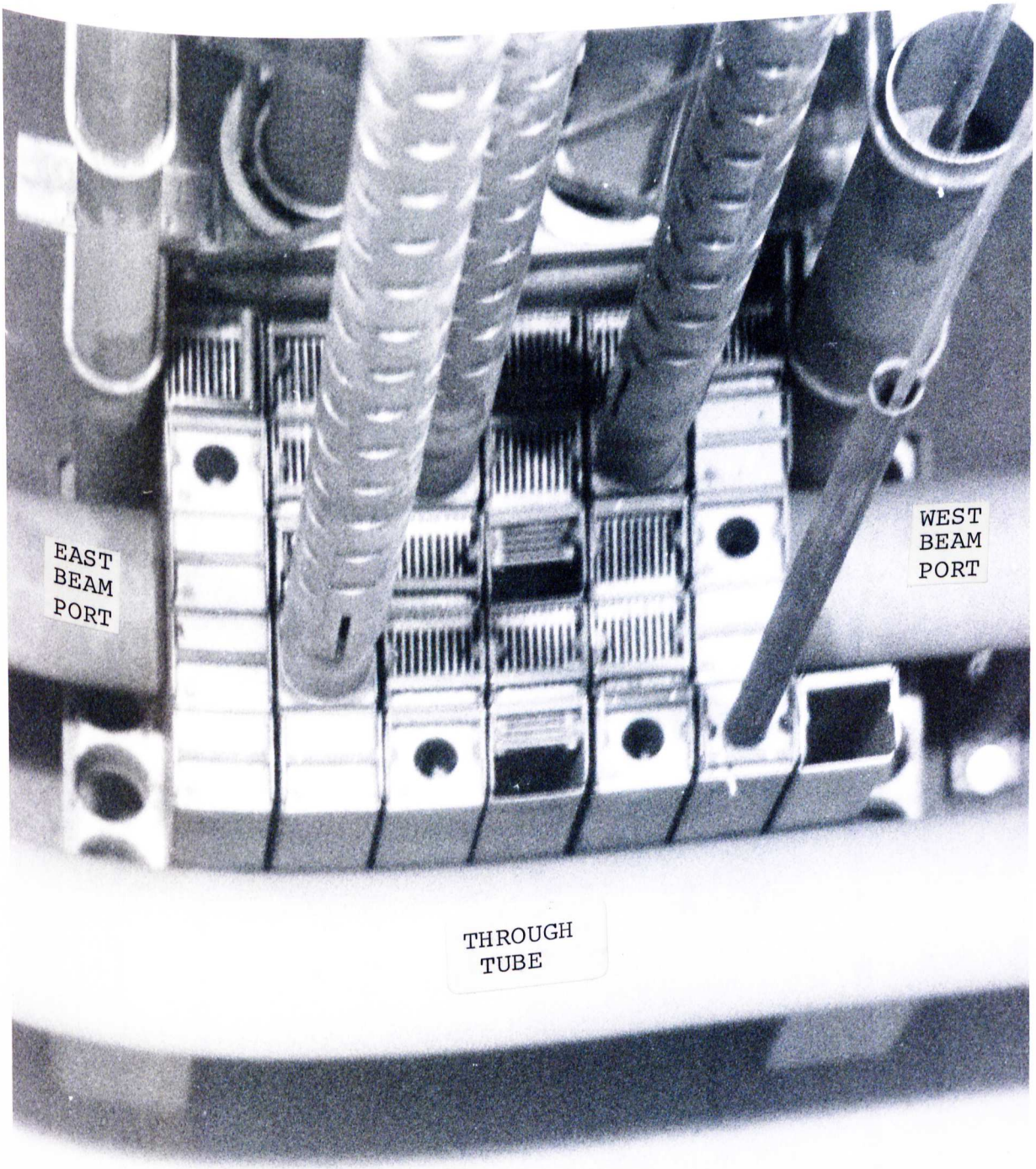

FIGURE III

REACTOR CORE AND COMPONENTS

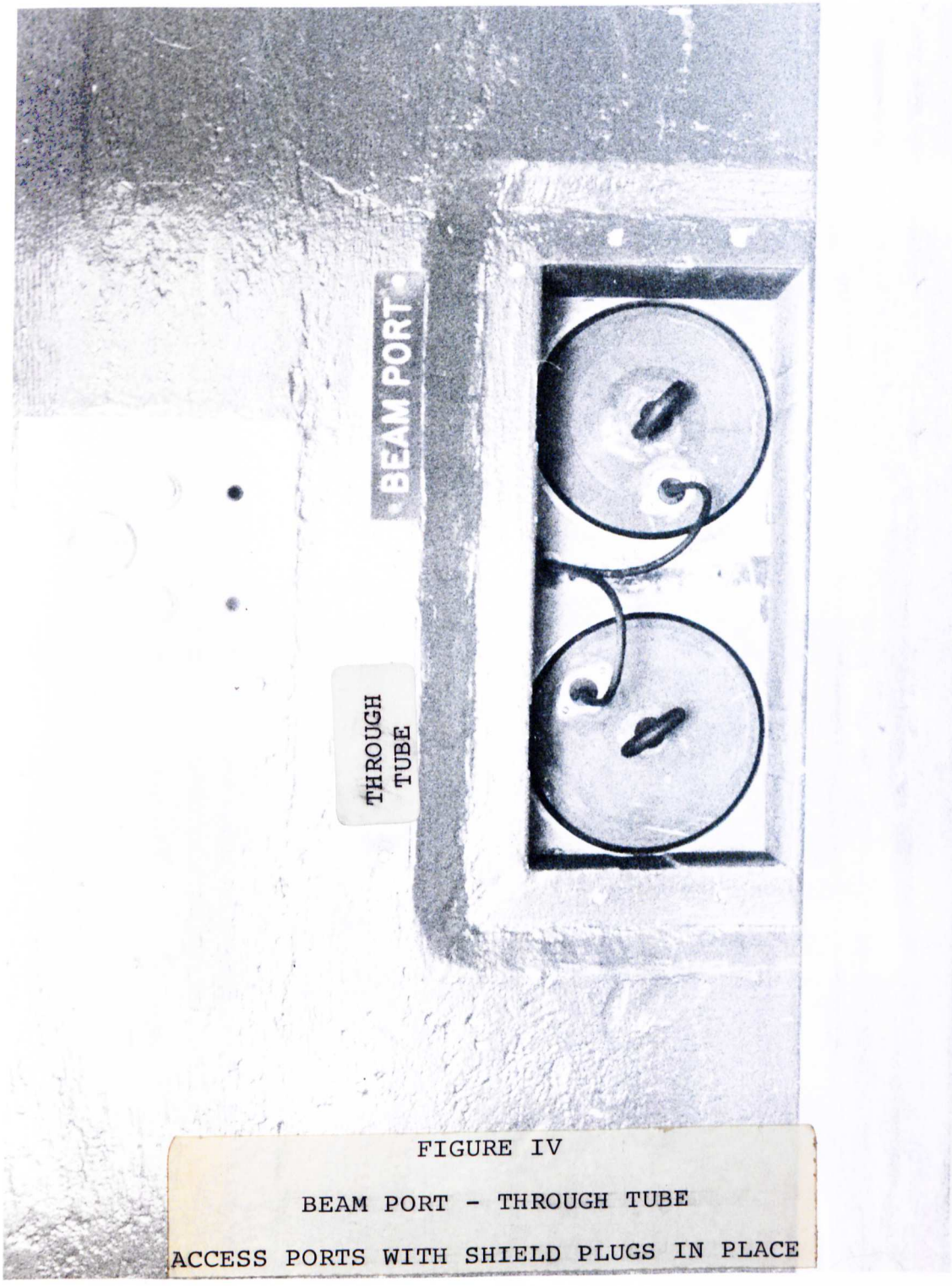

FIGURE IV

BEAM PORT - THROUGH TUBE

ACCESS PORTS WITH SHIELD PLUGS IN PLACE

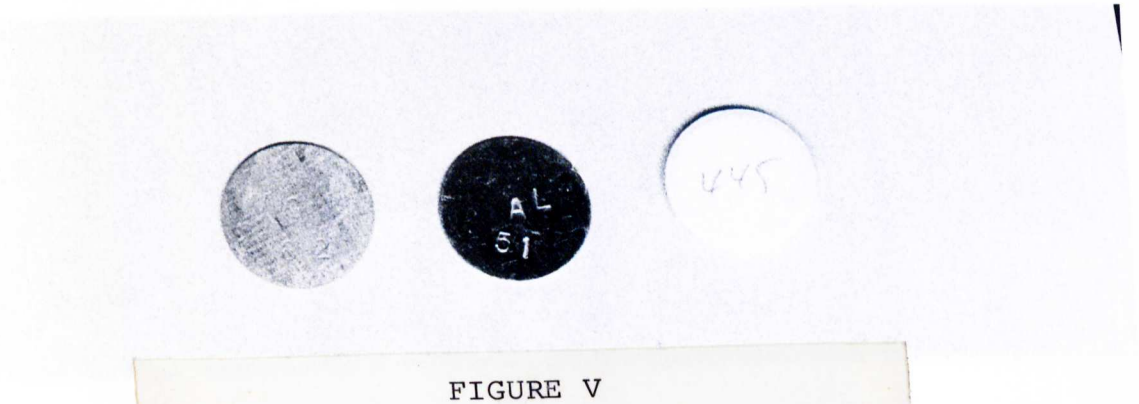

FIGURE V

SULFUR (#445), MAGNESIUM AND ALUMINUM

NEUTRON DOSIMETER FOILS

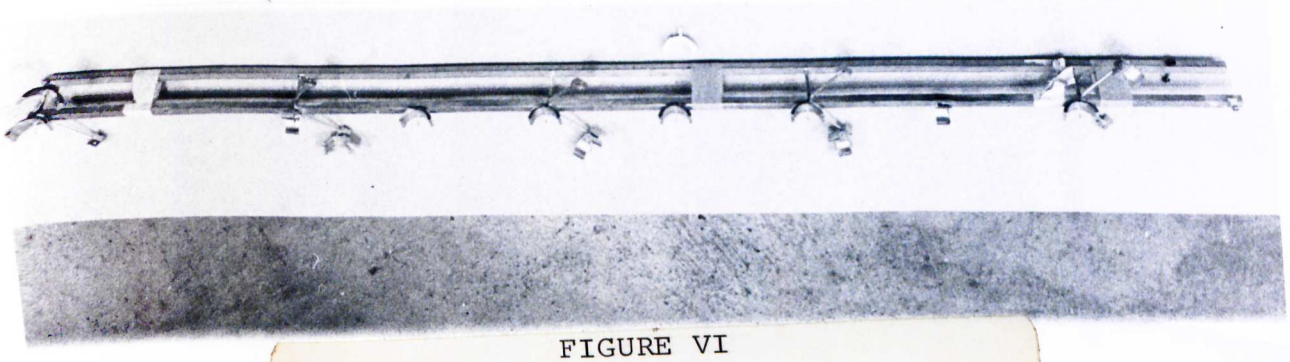

FIGURE VI

BEAM PORT - THROUGH TUBE

DOSIMETER SUPPORT JIG

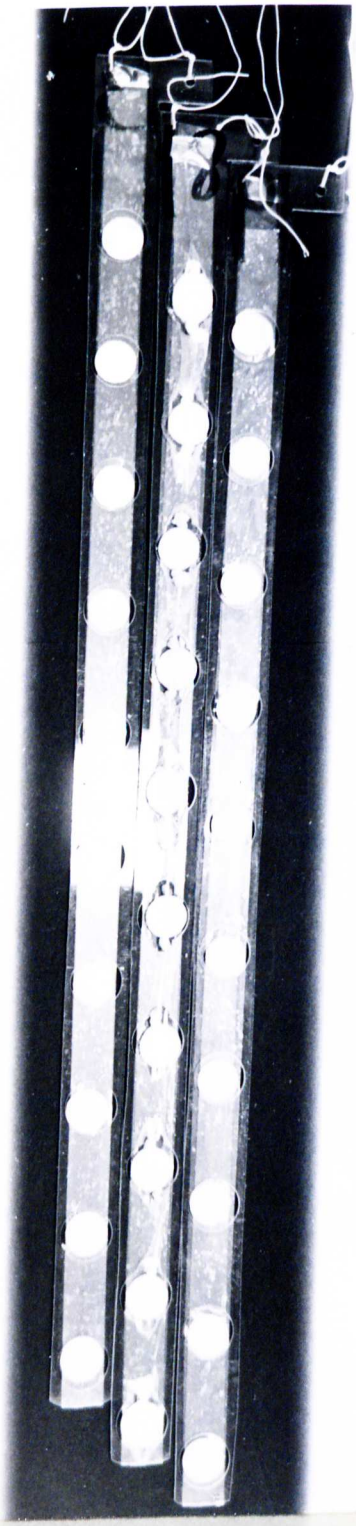

FIGURE VII

"GLORY HOLE" - FUEL ELEMENT

DOSIMETER SUPPORT STRIPS

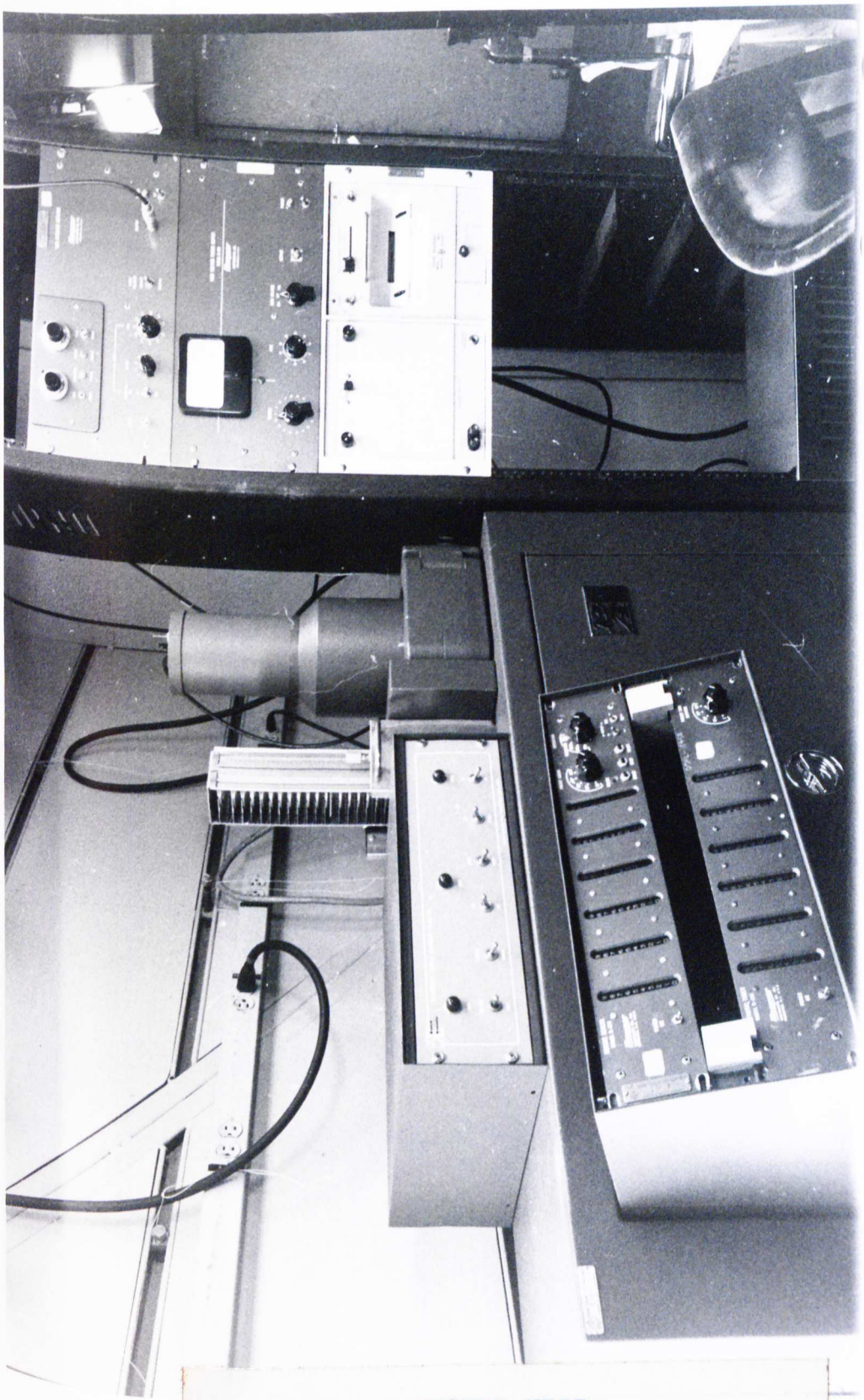

FIGURE VIII

DOSIMETER COUNTING SYSTEM

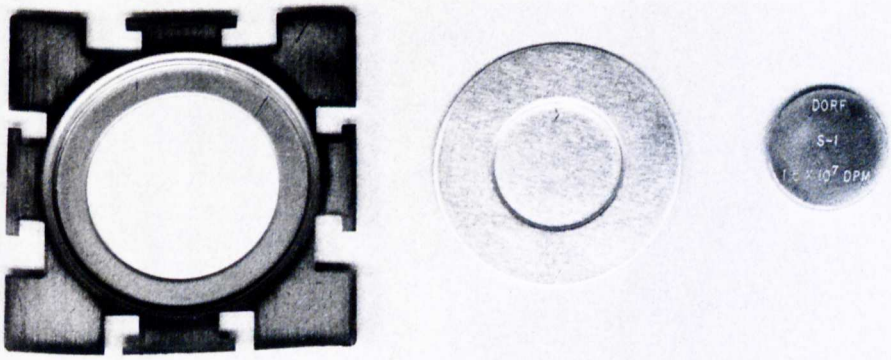

FIGURE IX

STANDARD SOURCE, PLANCHET,

AND PLANCHET HOLDER

AS USED IN THE BAIRD ATOMIC MODEL 750

AUTOMATIC SAMPLE CHANGER

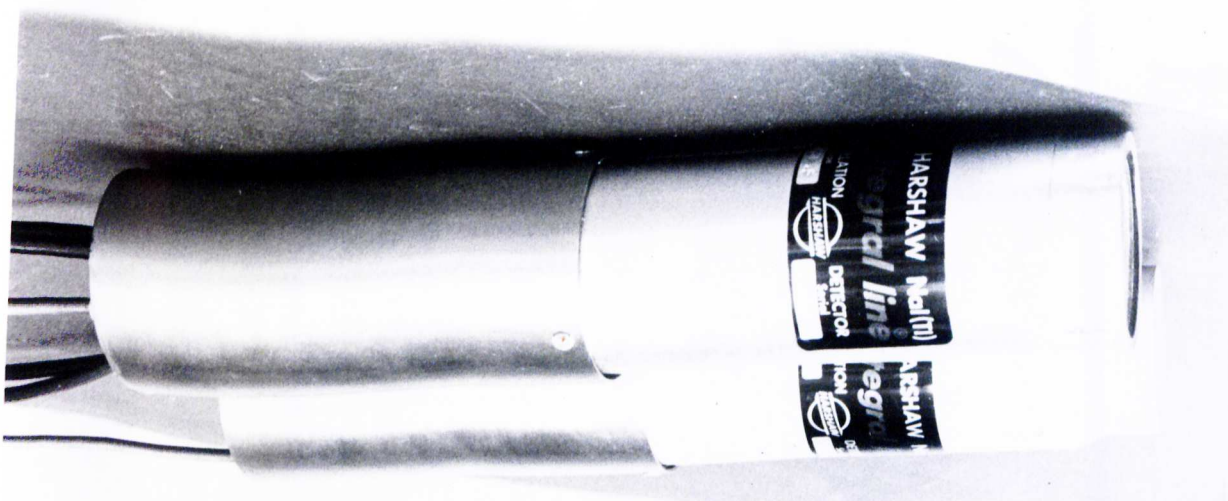

FIGURE X

β^- AND γ RAY SCINTILLATION

DETECTOR ASSEMBLIES

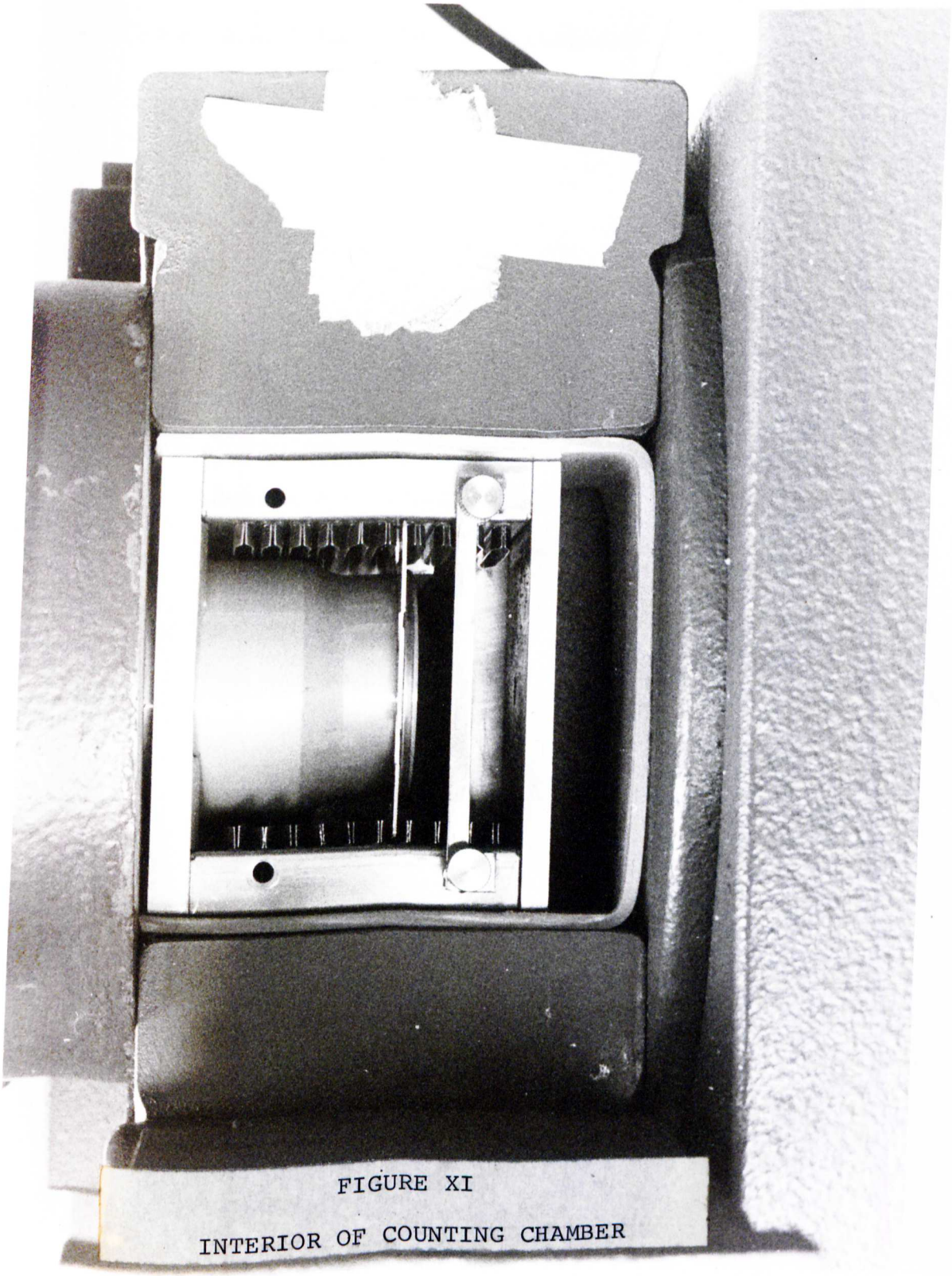

FIGURE XI

INTERIOR OF COUNTING CHAMBER

FIGURE 1

VERTICAL FAST NEUTRON FLUX DISTRIBUTION AT POSITION B-2

A TYPICAL IRRADIATION POSITION ADJACENT TO THE REFLECTOR

POWER LEVEL: 10 kw

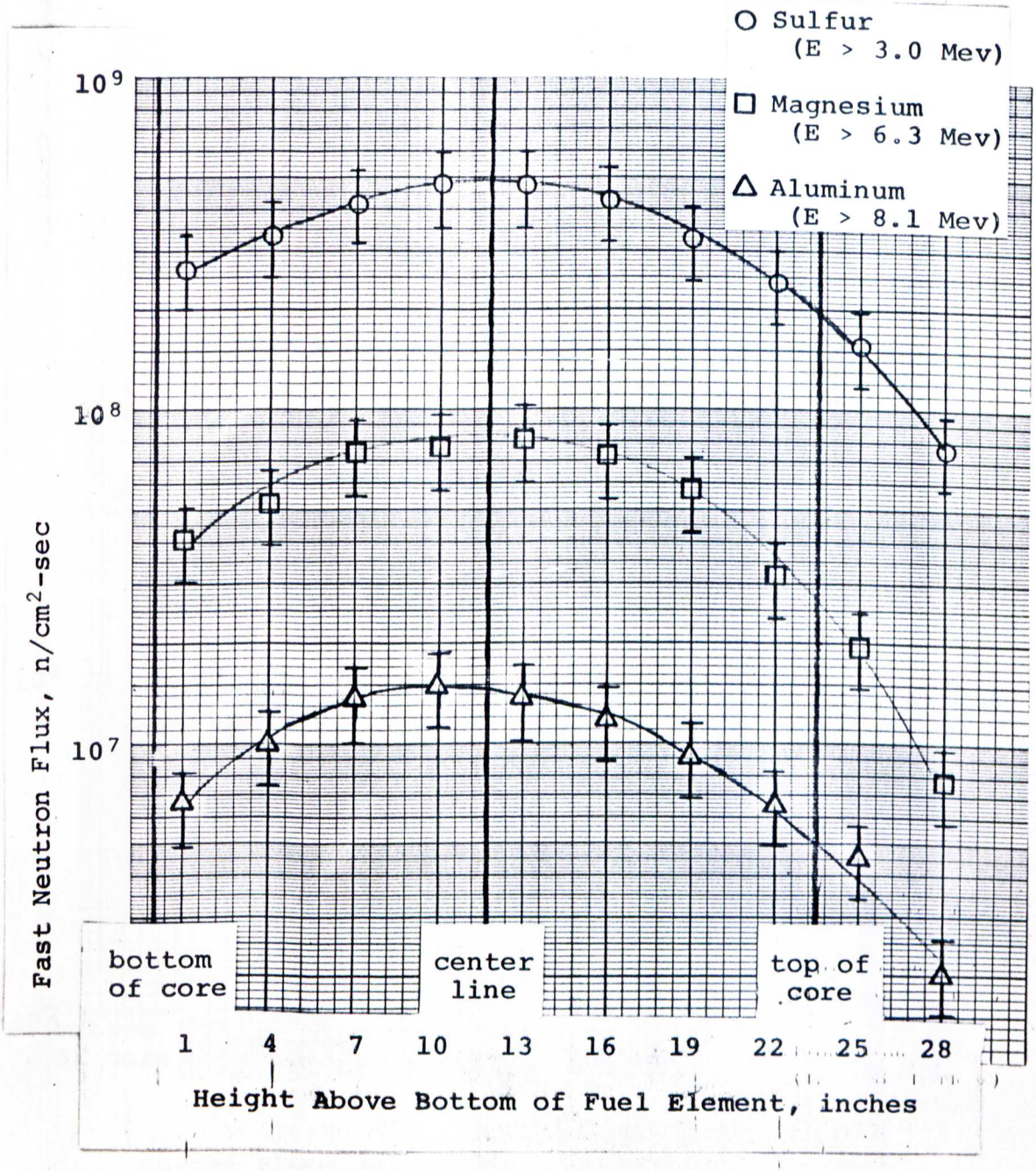

FIGURE 2

VERTICAL FAST NEUTRON FLUX DISTRIBUTION

IN THE OUTER "GLORY HOLE" - FUEL ELEMENT B-5

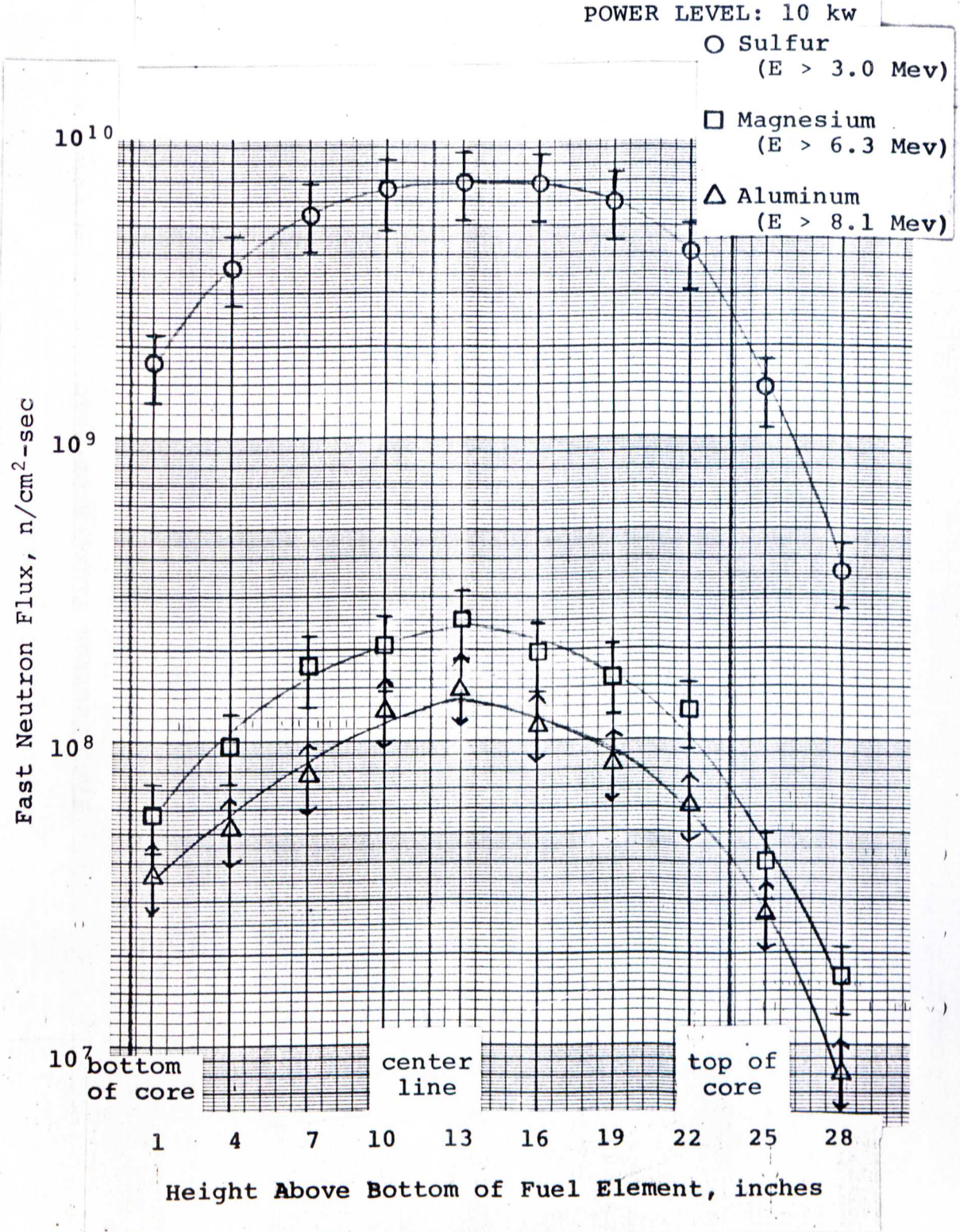

FIGURE 3

VERTICAL FAST NEUTRON FLUX DISTRIBUTION IN FUEL ELEMENT C-4

POWER LEVEL: 10 kw

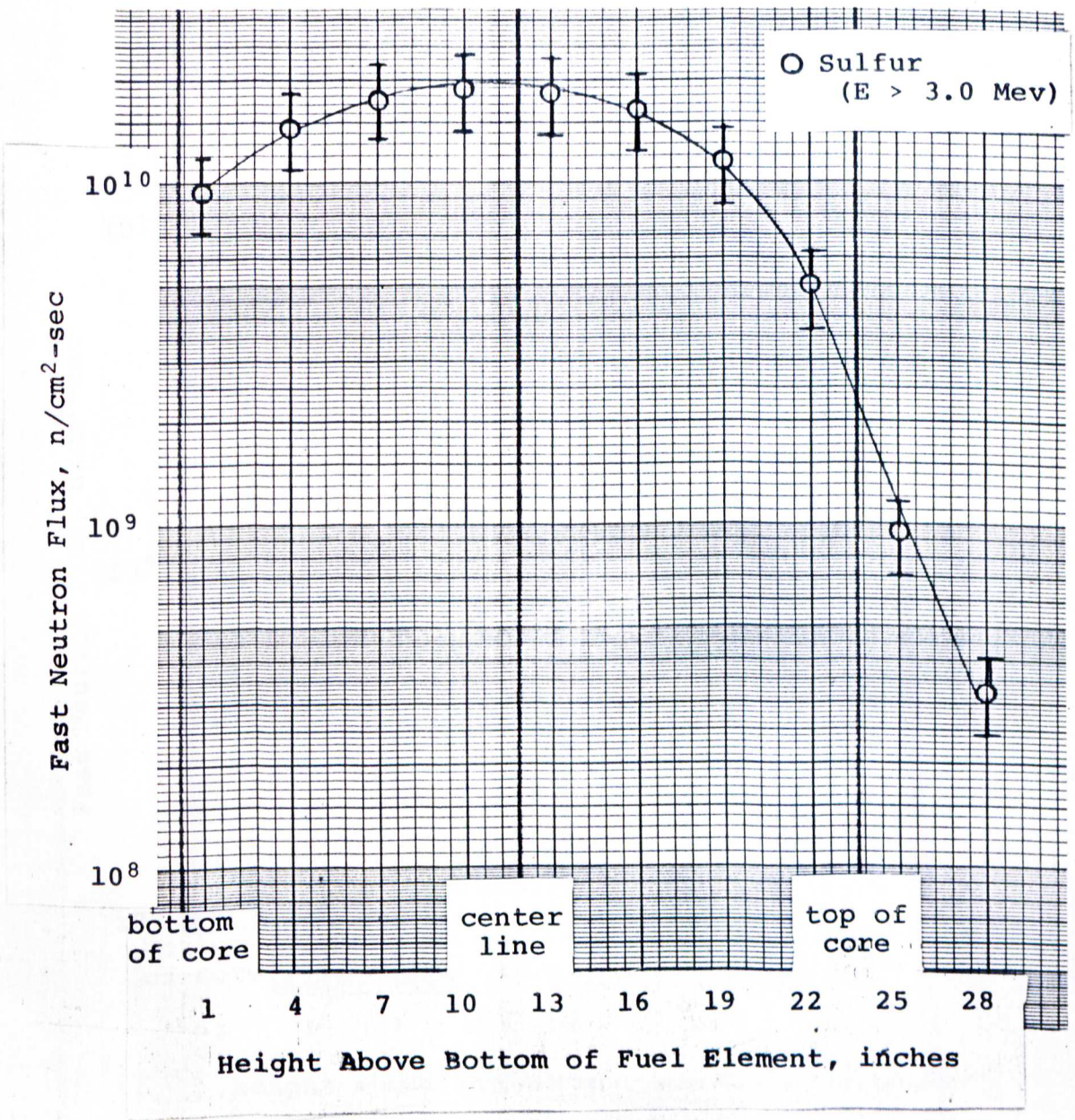

FIGURE 4

VERTICAL FAST NEUTRON FLUX DISTRIBUTION IN FUEL ELEMENT C-5

POWER LEVEL: 10 kw

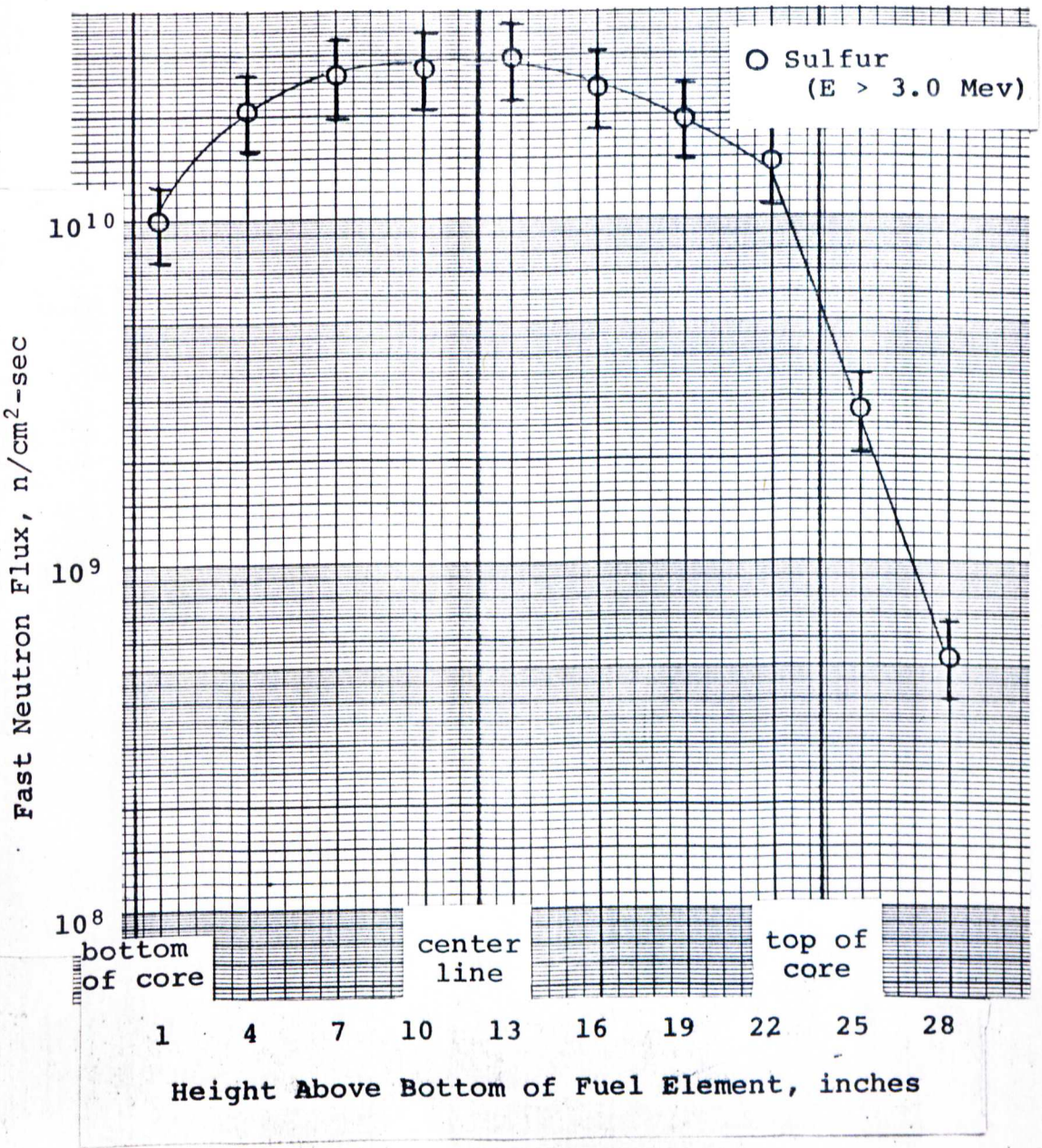

FIGURE 5

VERTICAL FAST NEUTRON FLUX DISTRIBUTION IN FUEL ELEMENT C-6

POWER LEVEL: 10 kw

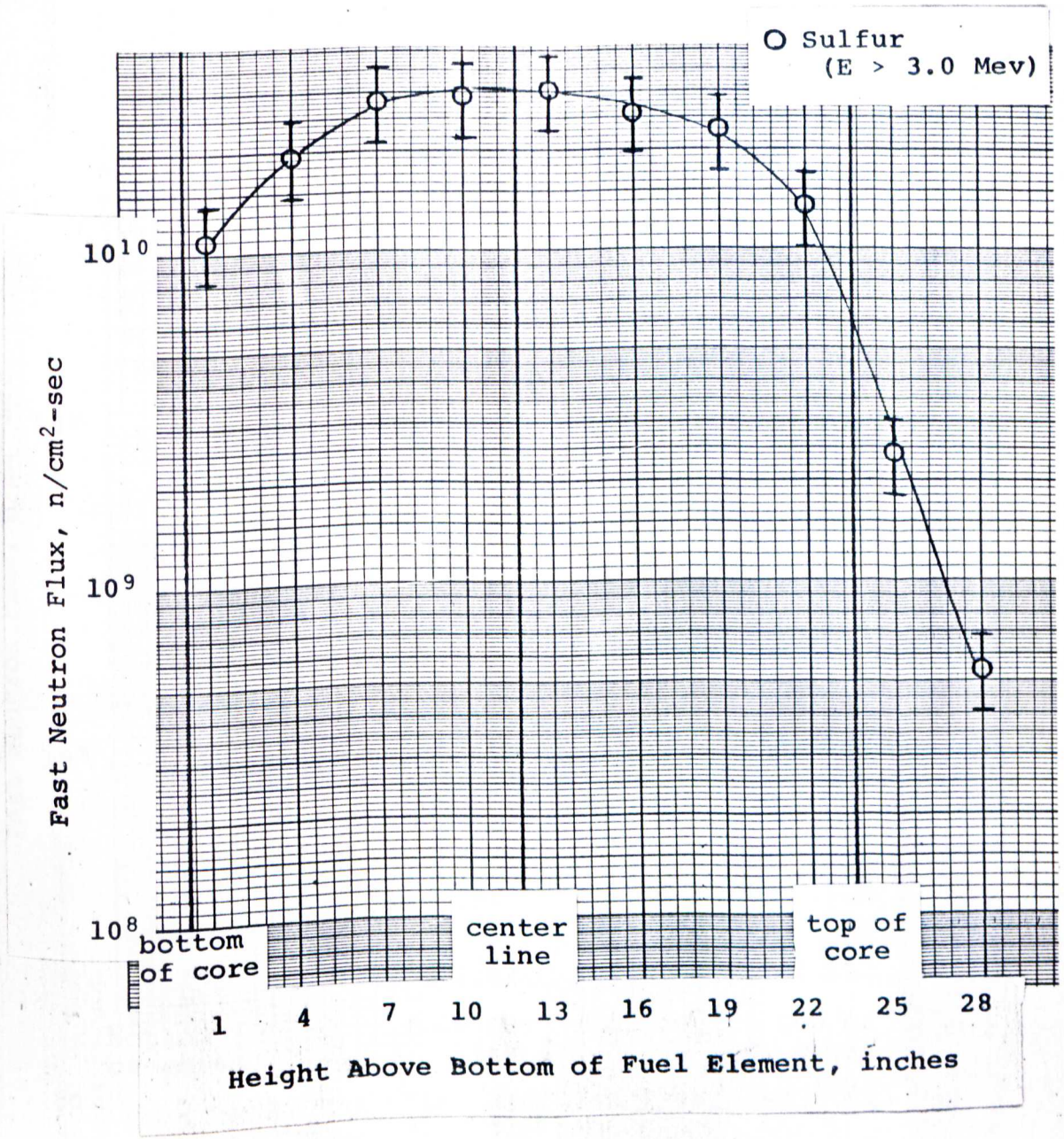

FIGURE 6

VERTICAL FAST NEUTRON FLUX DISTRIBUTION IN FUEL ELEMENT D-4

POWER LEVEL: 10 kw

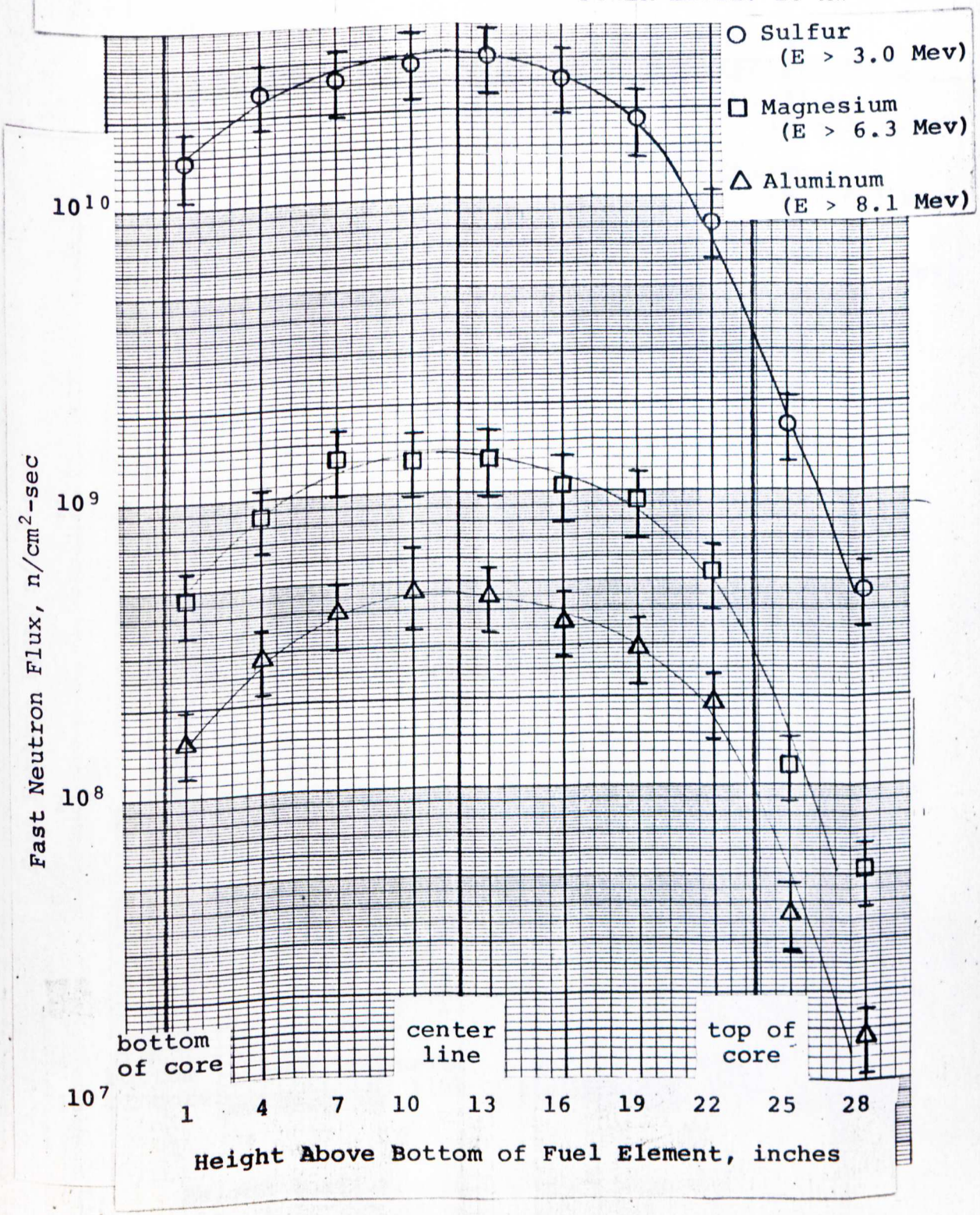

FIGURE 7

VERTICAL FAST NEUTRON FLUX DISTRIBUTION

IN THE CENTRAL "GLORY HOLE" - FUEL ELEMENT D-5

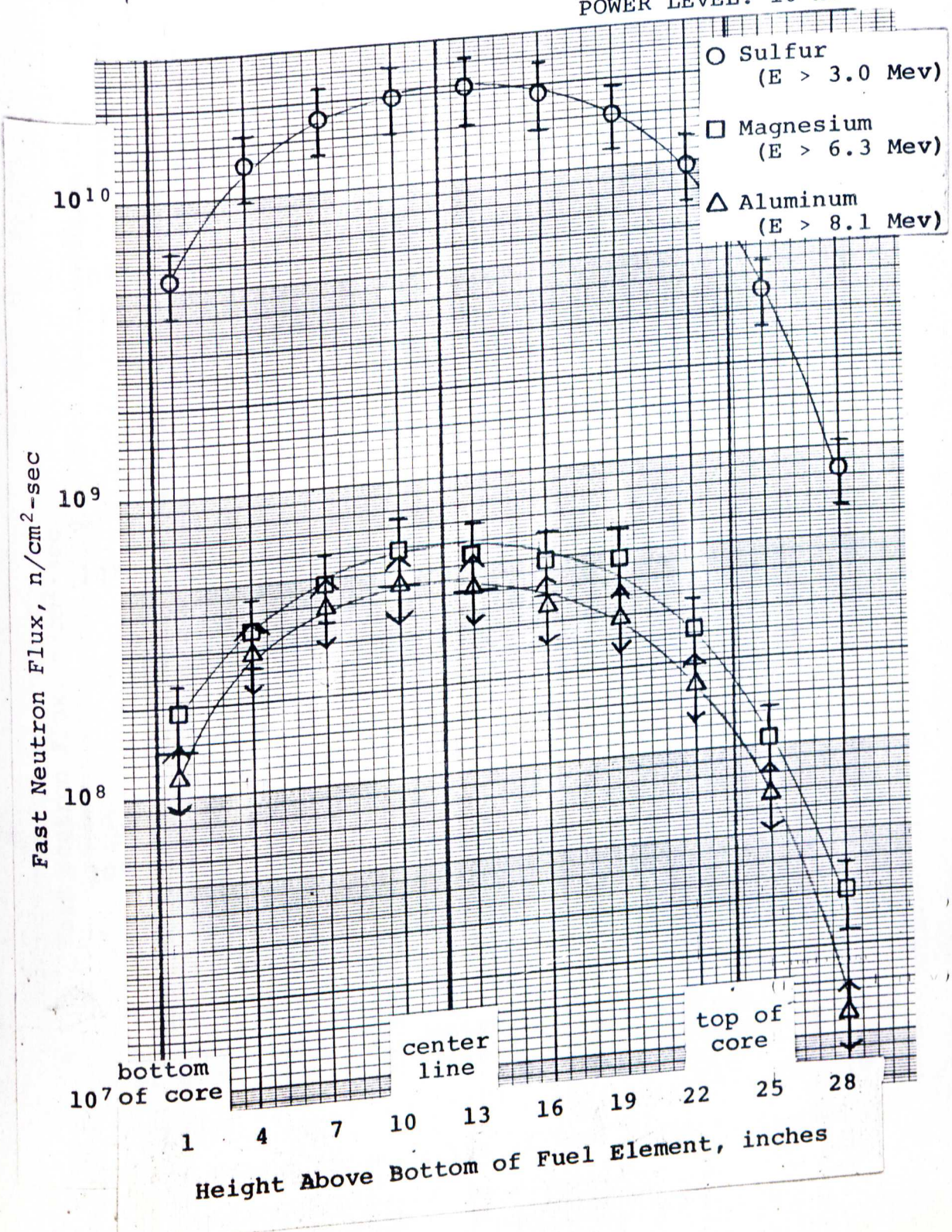

FIGURE 8

VERTICAL FAST NEUTRON FLUX DISTRIBUTION IN FUEL ELEMENT D-6

POWER LEVEL: 10 kw

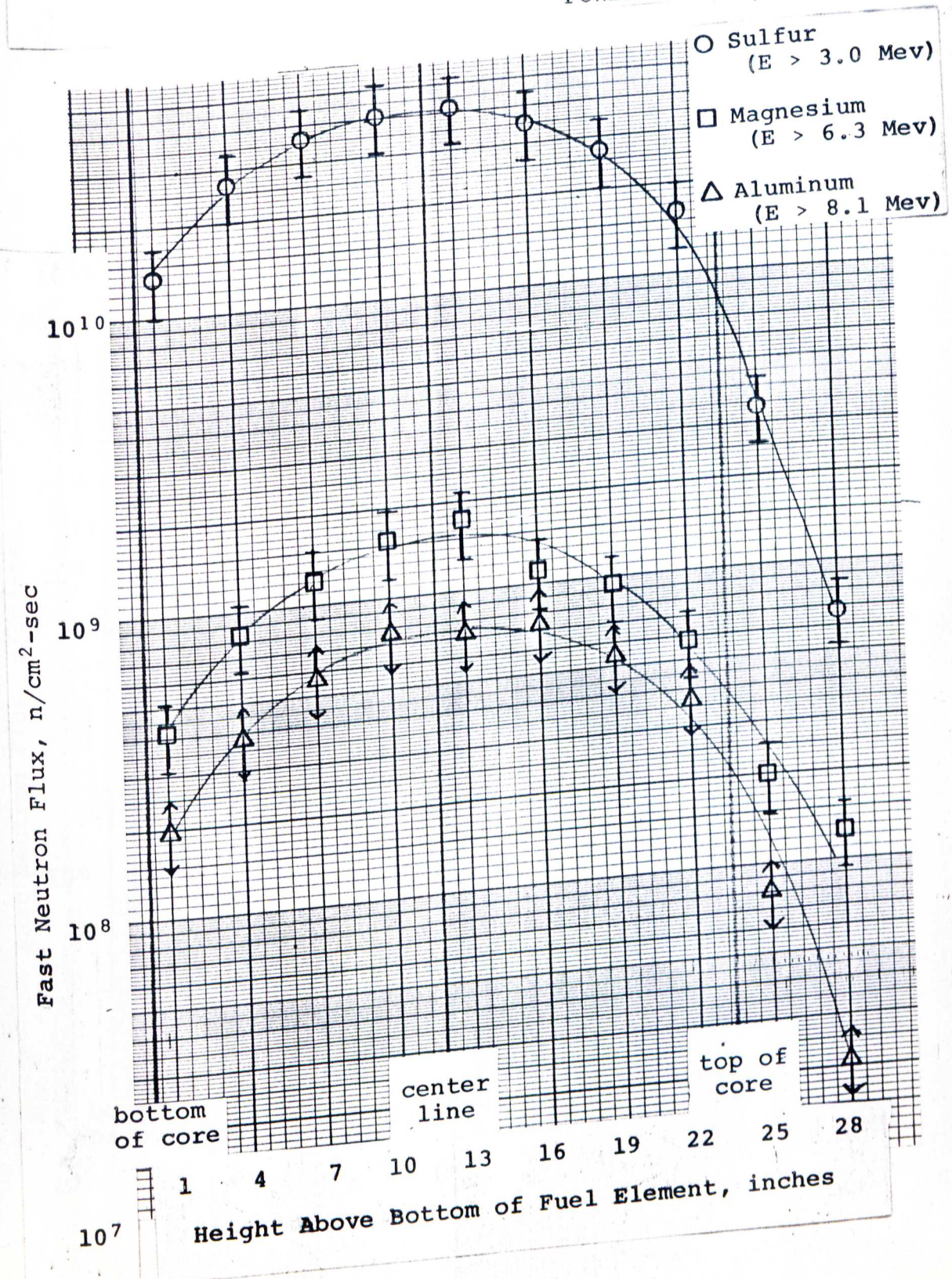

FIGURE 9

VERTICAL FAST NEUTRON FLUX DISTRIBUTION IN FUEL ELEMENT D-7

POWER LEVEL: 10 kw

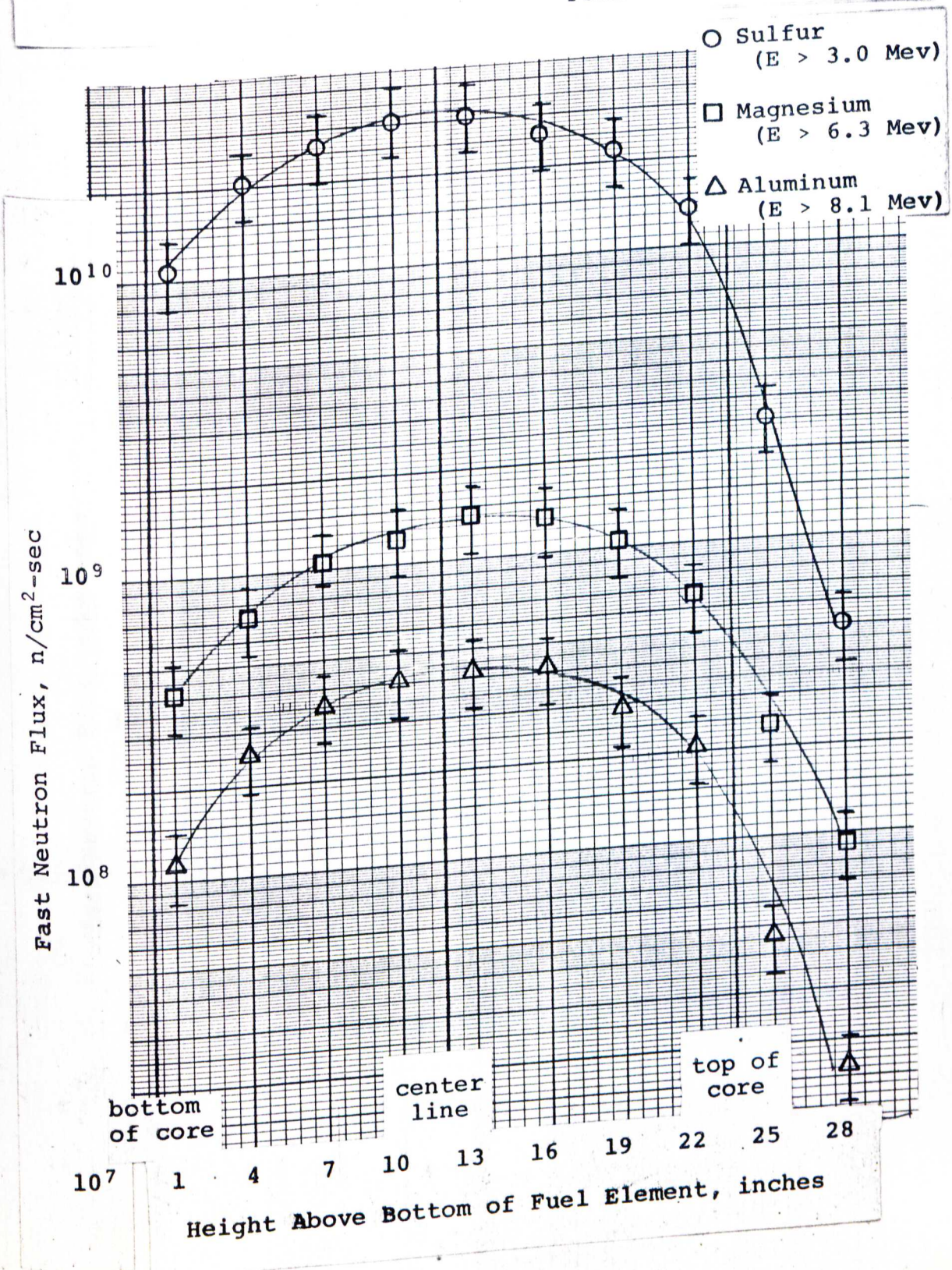

FIGURE 10

VERTICAL FAST NEUTRON FLUX DISTRIBUTION IN FUEL ELEMENT E-5

POWER LEVEL: 10 kw

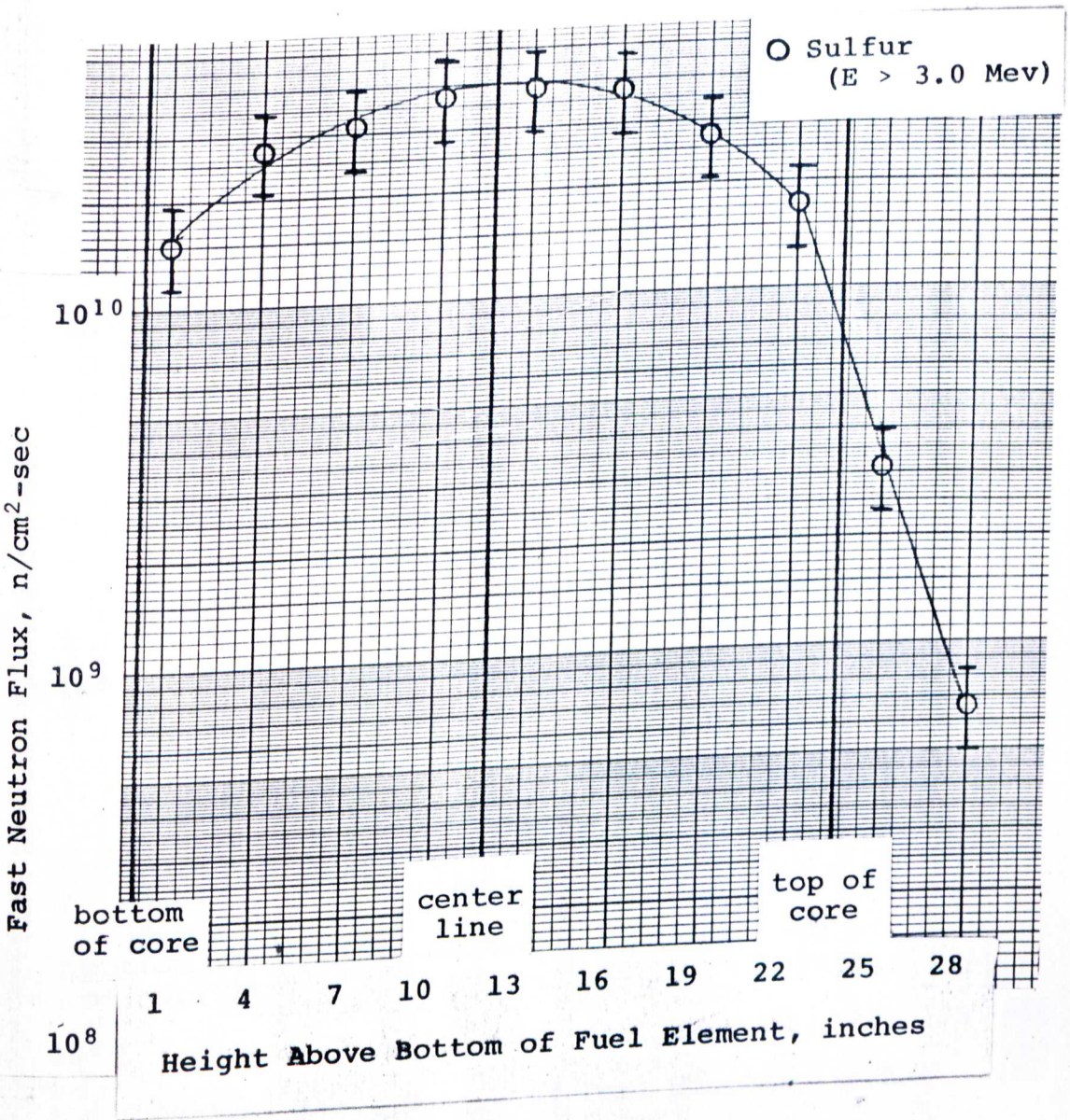

FIGURE 11

VERTICAL FAST NEUTRON FLUX DISTRIBUTION IN FUEL ELEMENT E-7

POWER LEVEL: 10 kw

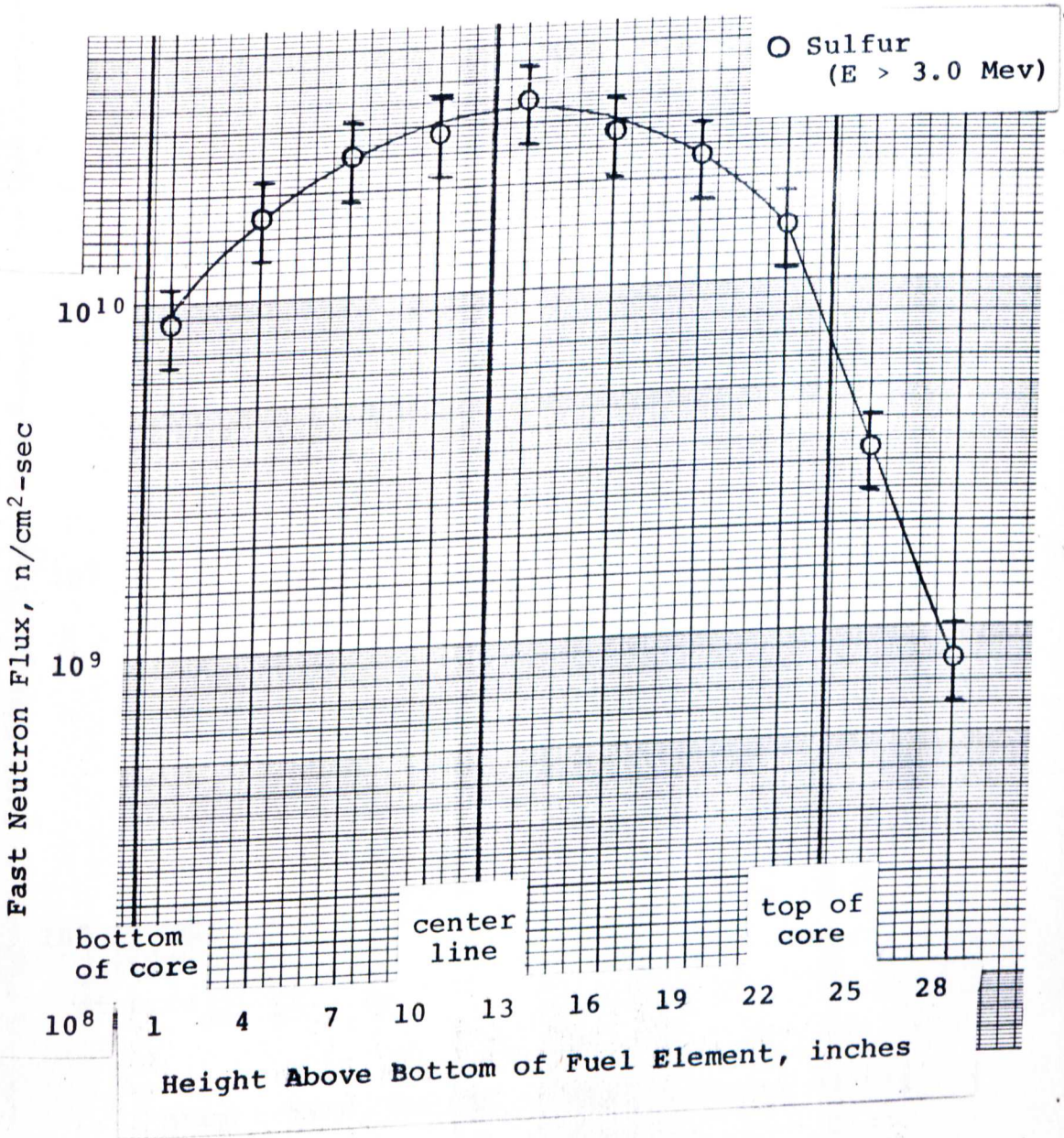

FIGURE 12

VERTICAL FAST NEUTRON FLUX DISTRIBUTION IN FUEL ELEMENT F-3

POWER LEVEL: 10 kw

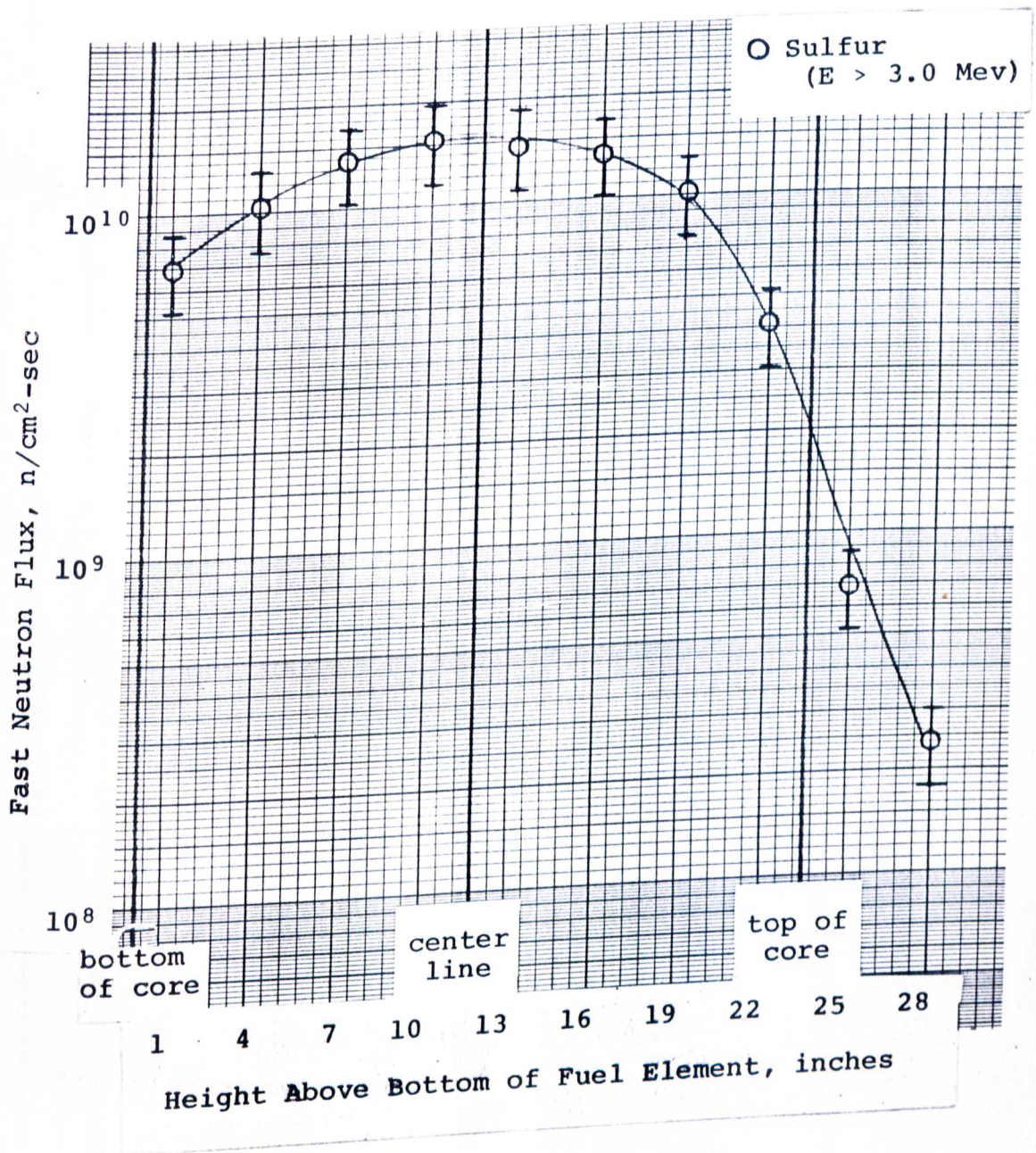

FIGURE 13

VERTICAL FAST NEUTRON FLUX DISTRIBUTION IN FUEL ELEMENT F-4

POWER LEVEL: 10 kw

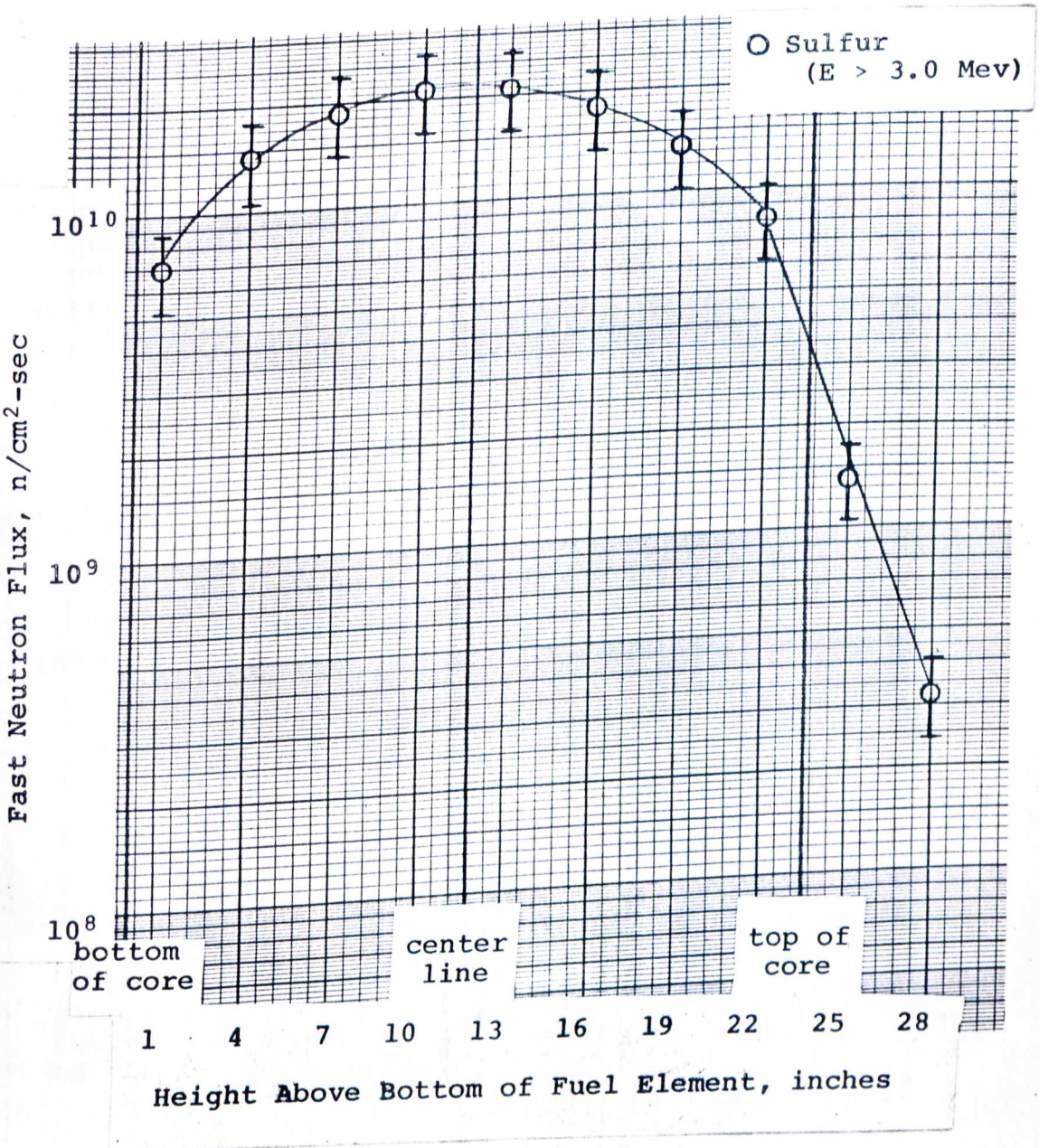

FIGURE 14

VERTICAL FAST NEUTRON FLUX DISTRIBUTION IN FUEL ELEMENT F-5

POWER LEVEL: 10 kw

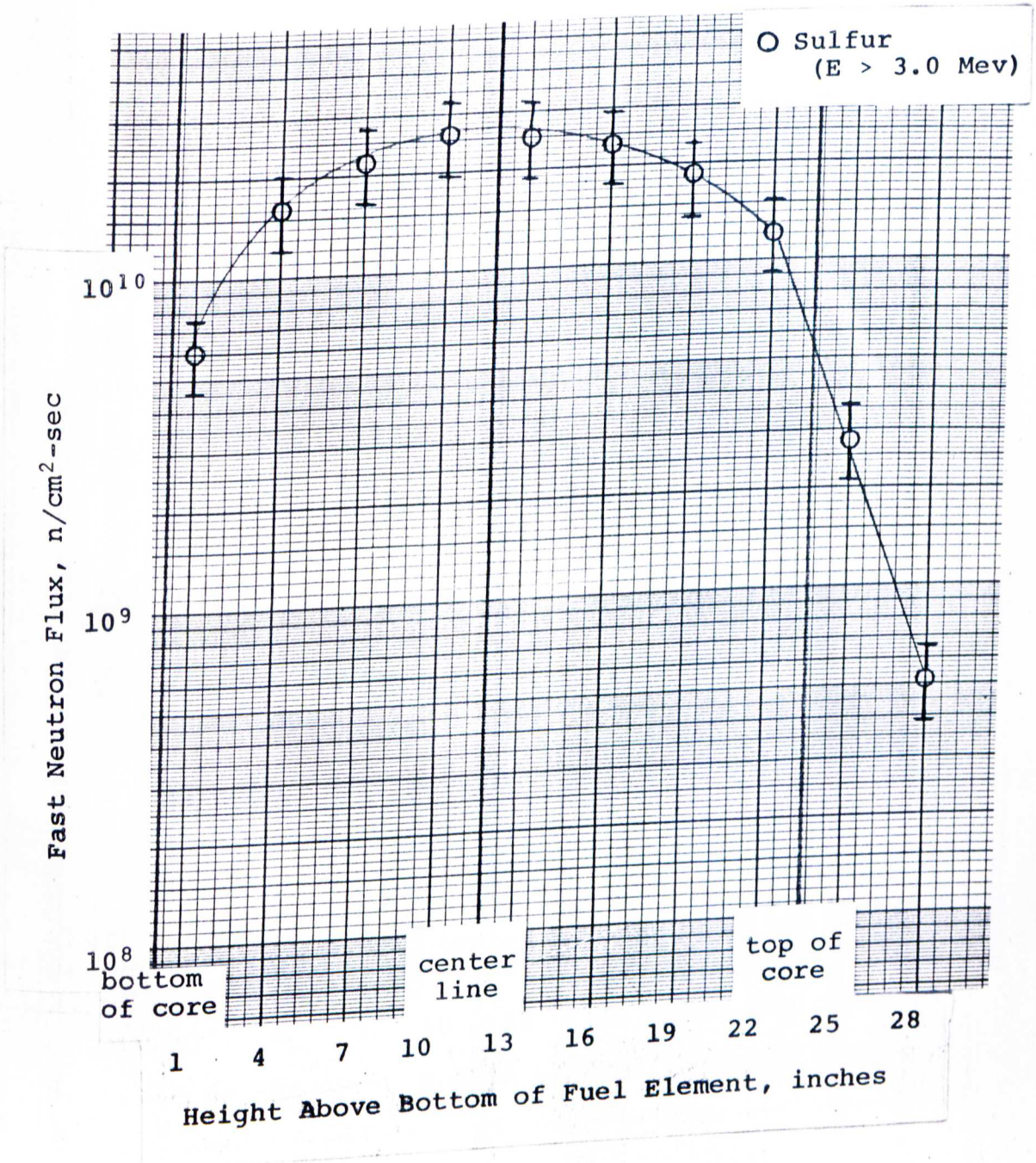

FIGURE 15

VERTICAL FAST NEUTRON FLUX DISTRIBUTION IN FUEL ELEMENT F-6

POWER LEVEL: 10 kw

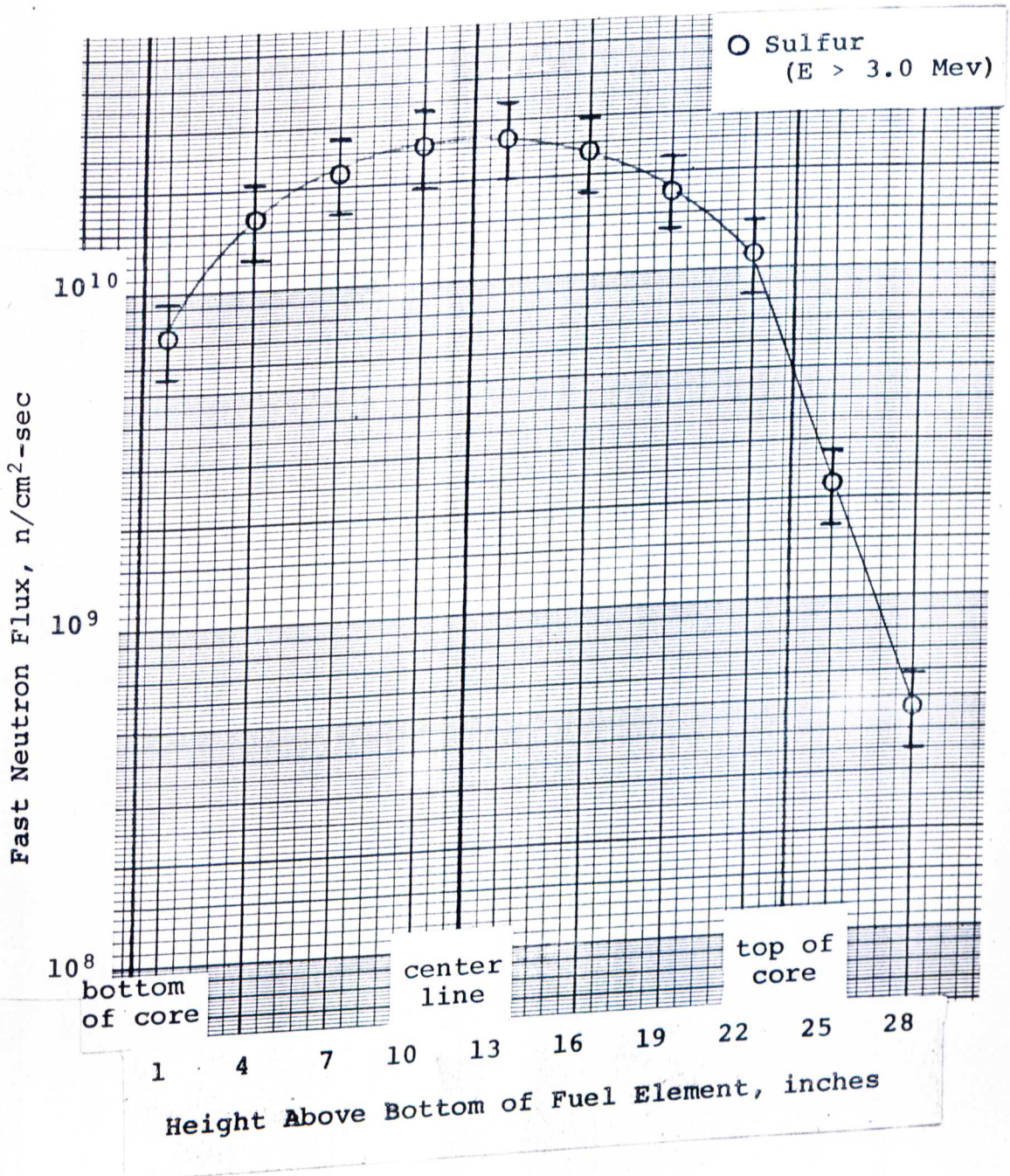

FIGURE 16

VERTICAL FAST NEUTRON FLUX DISTRIBUTION IN FUEL ELEMENT F-7

POWER LEVEL: 10 kw

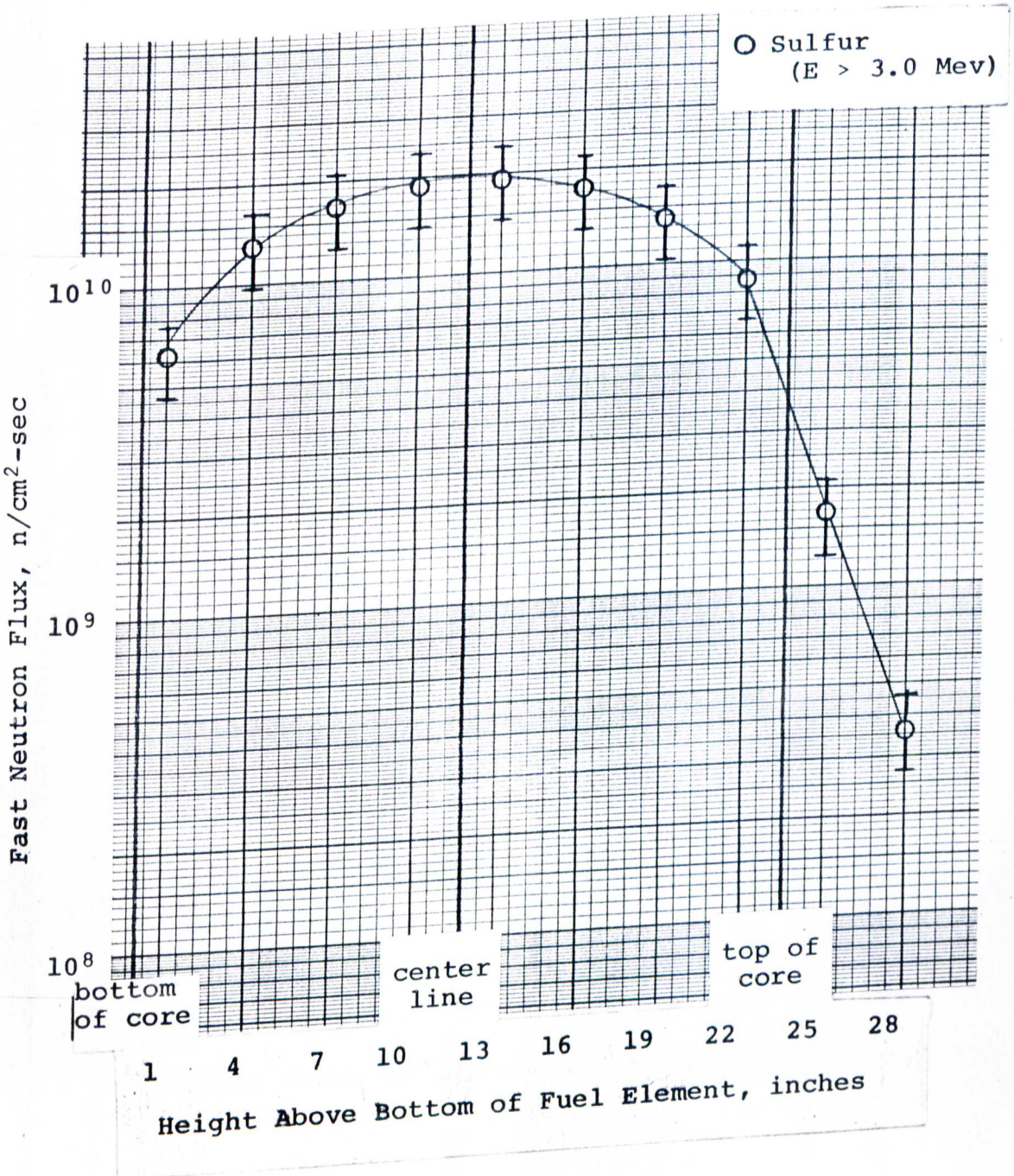

FIGURE 17

VERTICAL FAST NEUTRON FLUX DISTRIBUTION IN FUEL ELEMENT F-8

POWER LEVEL: 10 kw

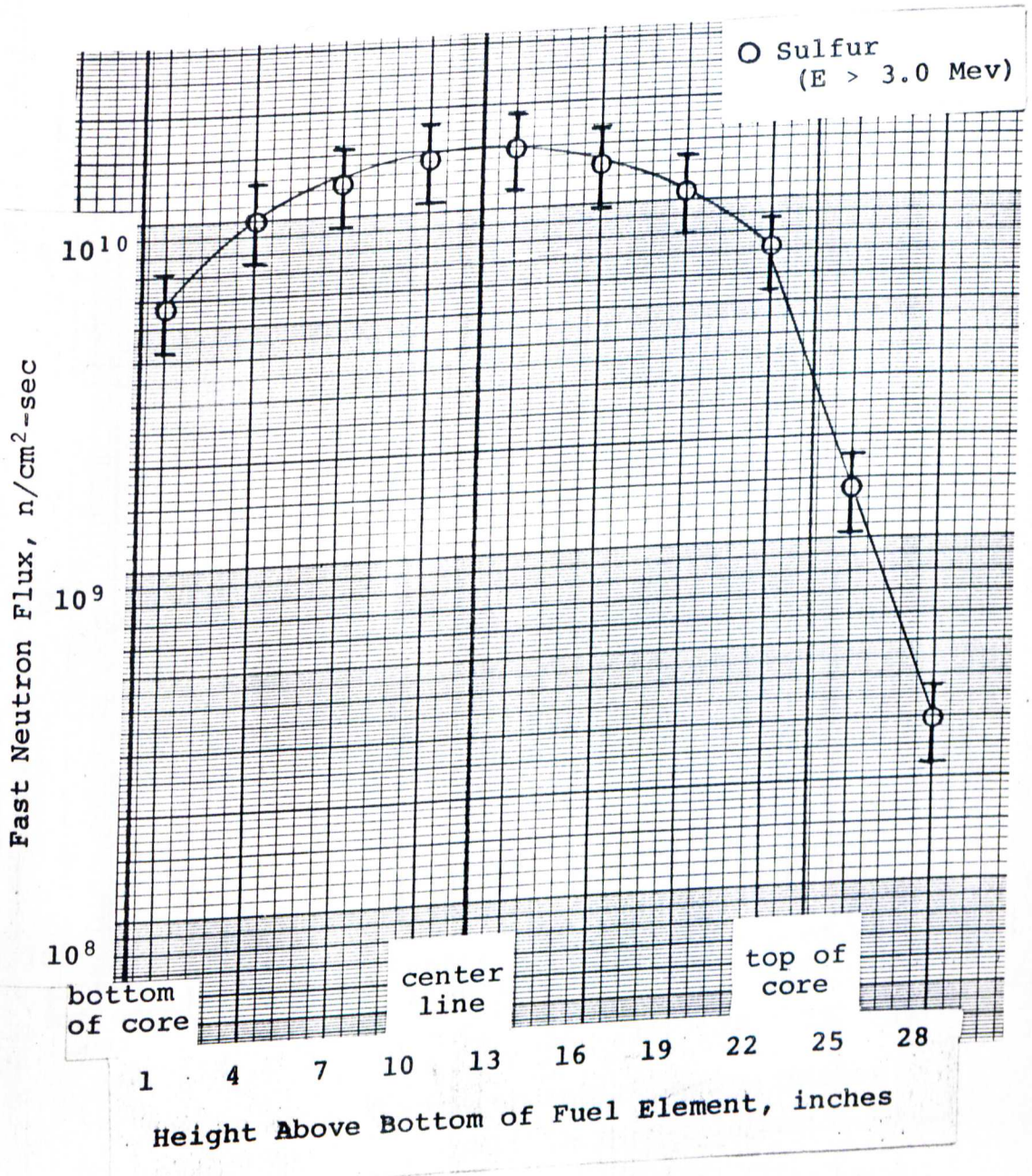

FIGURE 18

VERTICAL FAST NEUTRON FLUX DISTRIBUTION

IN FUEL ELEMENT D-6 - CONTROL ROD SHIM #2 WITHDRAWN

POWER LEVEL: 10 kw

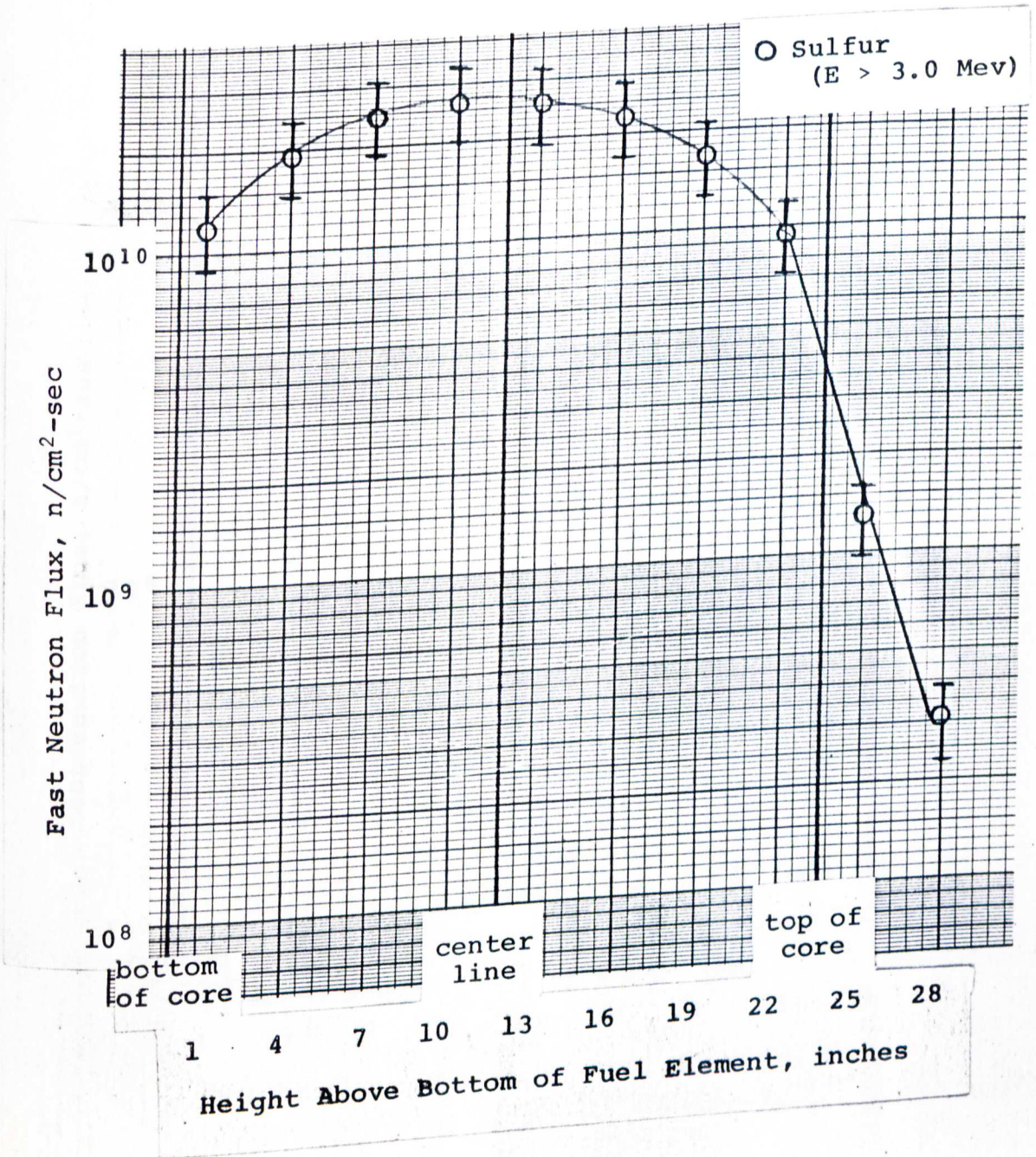

FIGURE 19

VERTICAL FAST NEUTRON FLUX DISTRIBUTION

IN FUEL ELEMENT E-5 - CONTROL ROD SHIM #2 WITHDRAWN

POWER LEVEL: 10 kw

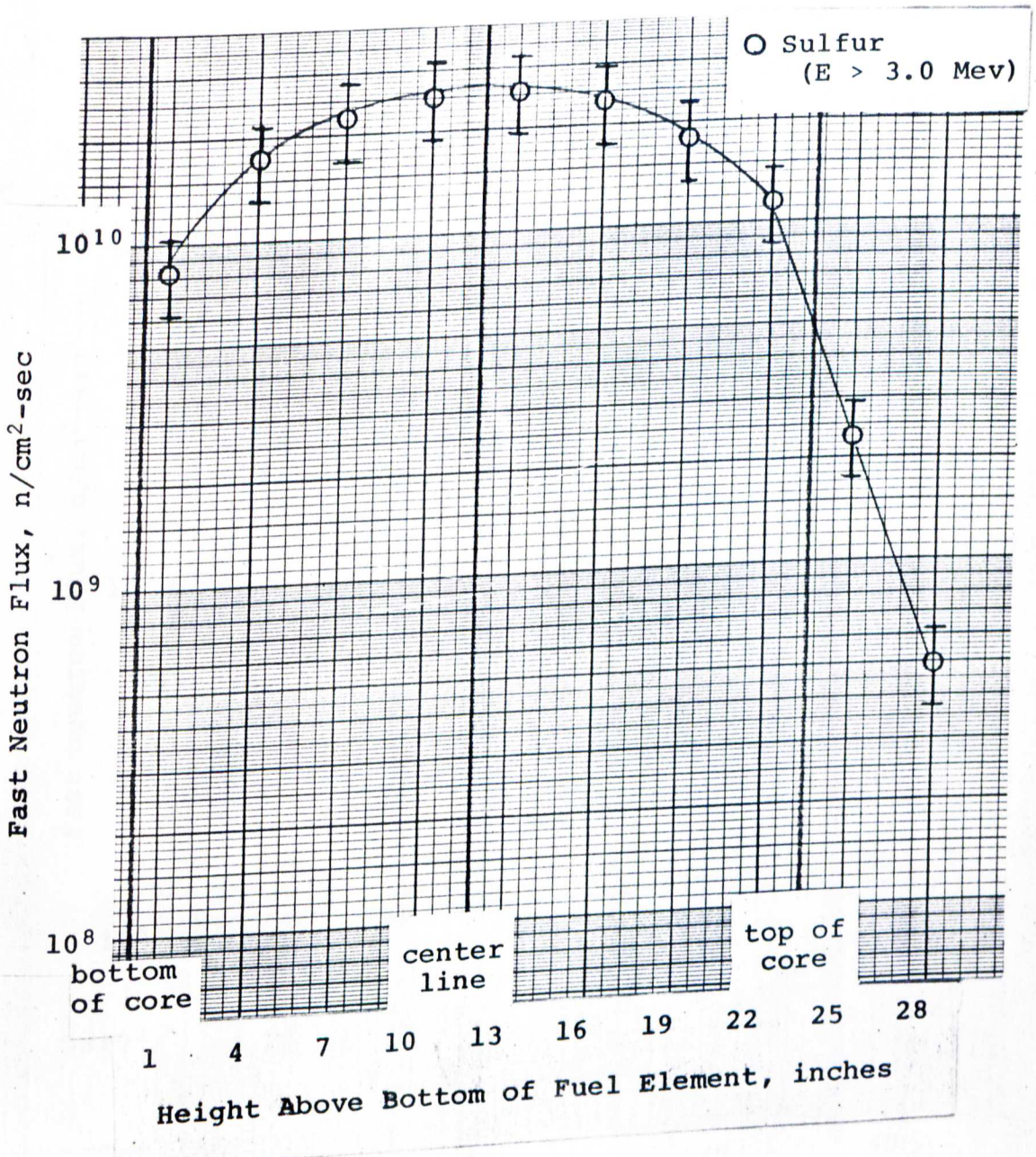

FIGURE 20

FAST NEUTRON FLUX DISTRIBUTION

ON LONGITUDINAL AXIS OF WEST BEAM PORT

POWER LEVEL: 10 kw

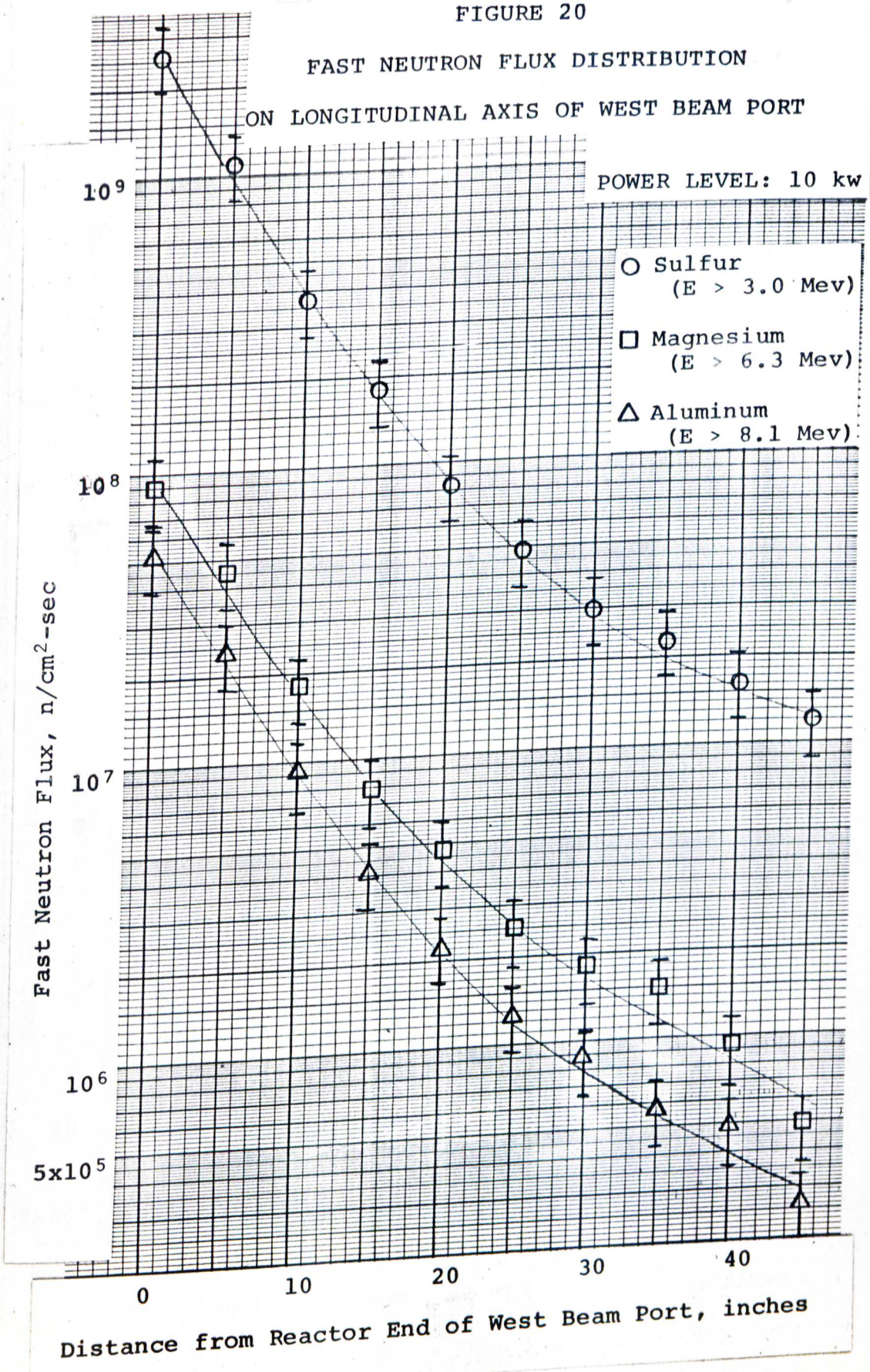

FIGURE 21

FAST NEUTRON FLUX DISTRIBUTION

ADJACENT TO NORTH WALL OF WEST BEAM PORT

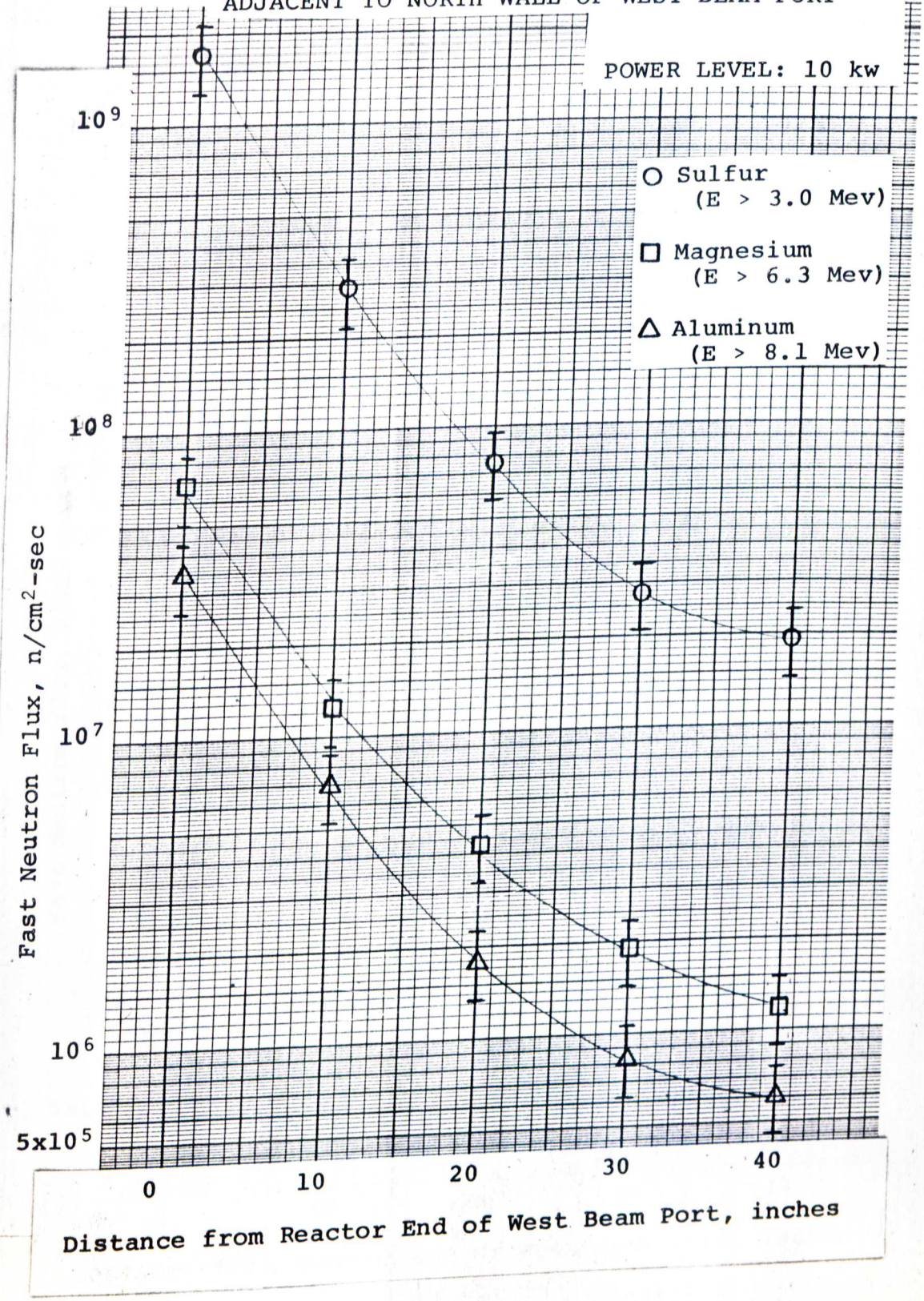

FIGURE 22

FAST NEUTRON FLUX DISTRIBUTION

ADJACENT TO SOUTH WALL OF WEST BEAM PORT

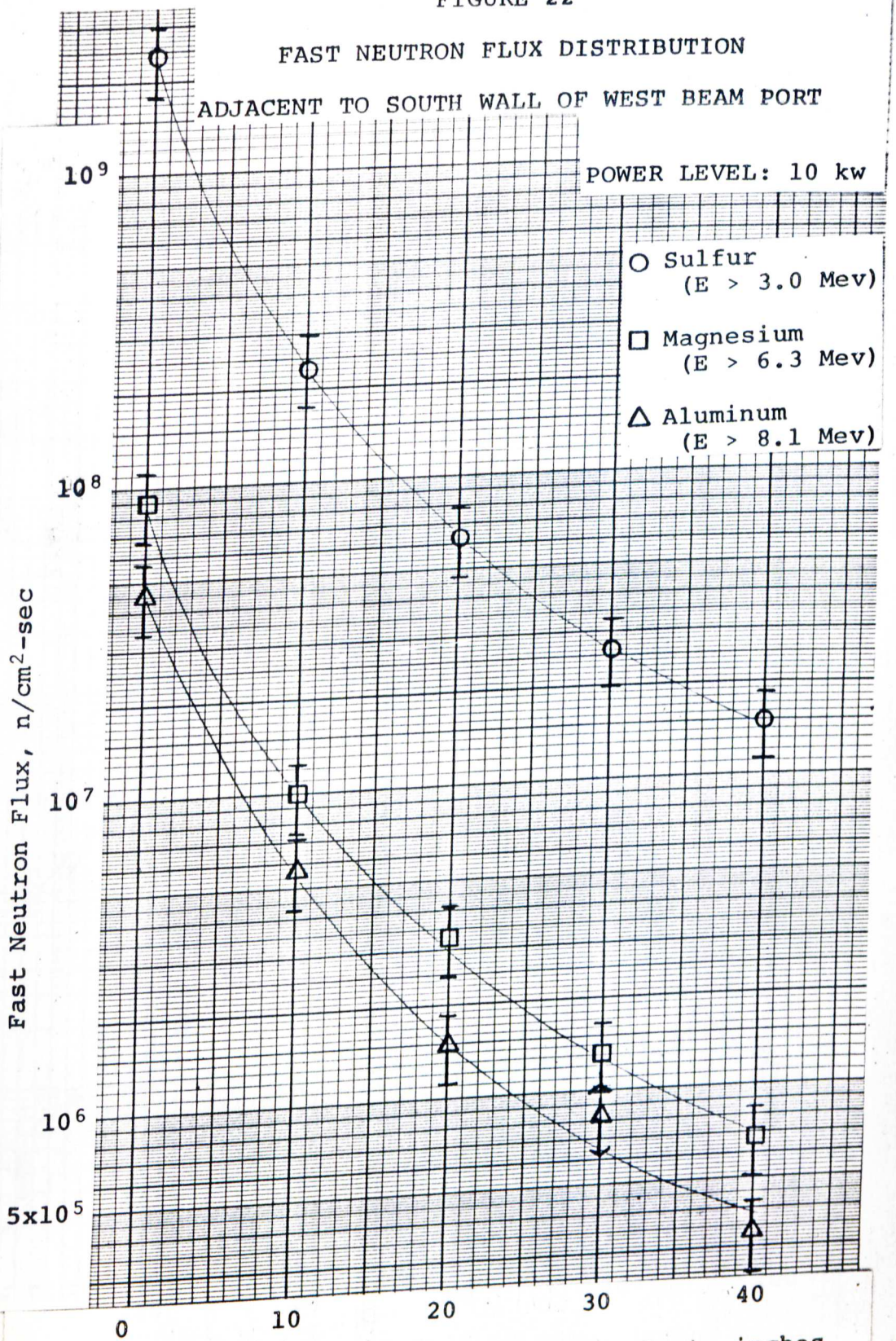

FIGURE 23

FAST NEUTRON FLUX DISTRIBUTION

ON LONGITUDINAL AXIS OF THROUGH TUBE

POWER LEVEL: 10 kw

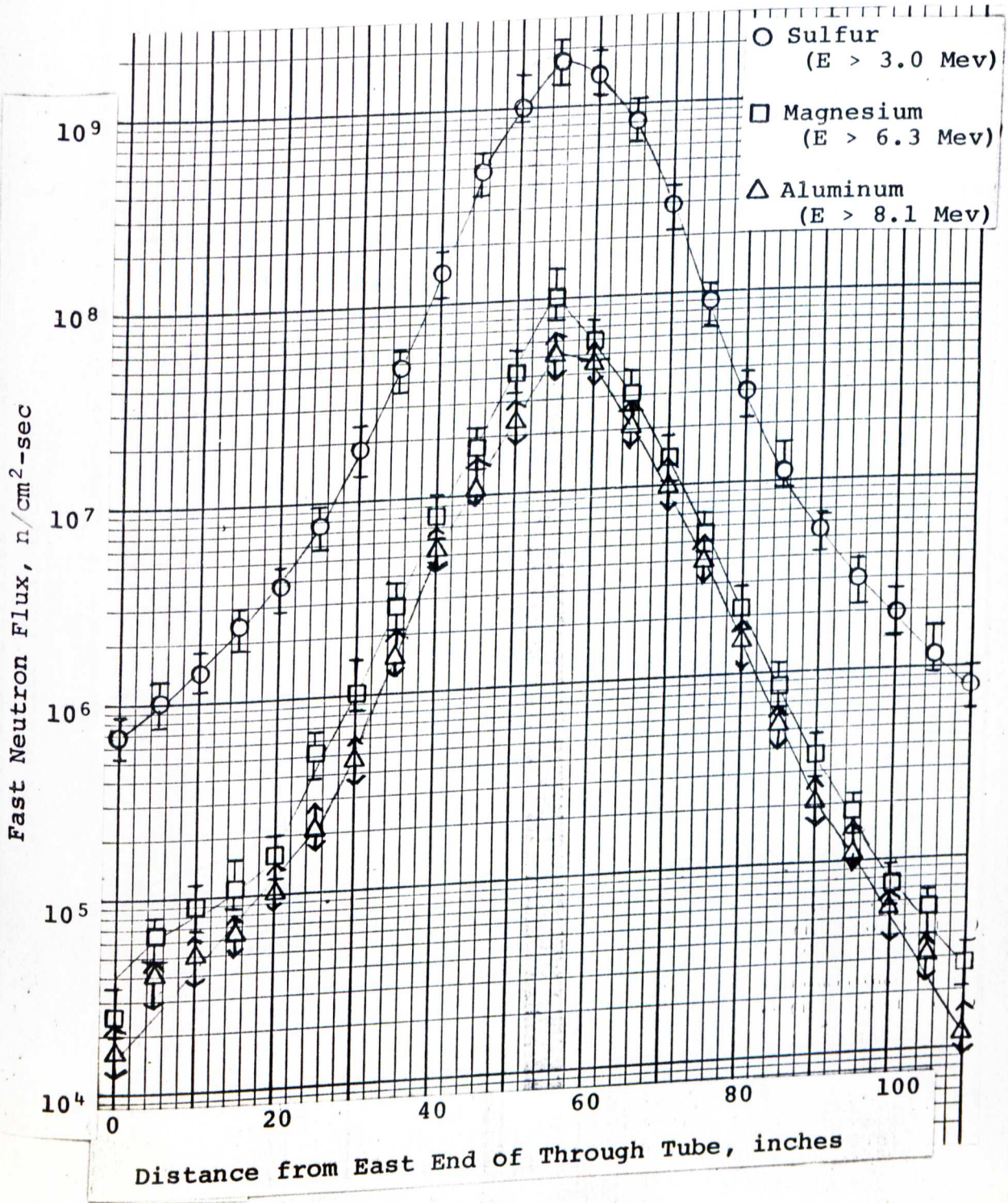

FIGURE 24

FAST NEUTRON FLUX DISTRIBUTION

ADJACENT TO SOUTH WALL OF THROUGH TUBE

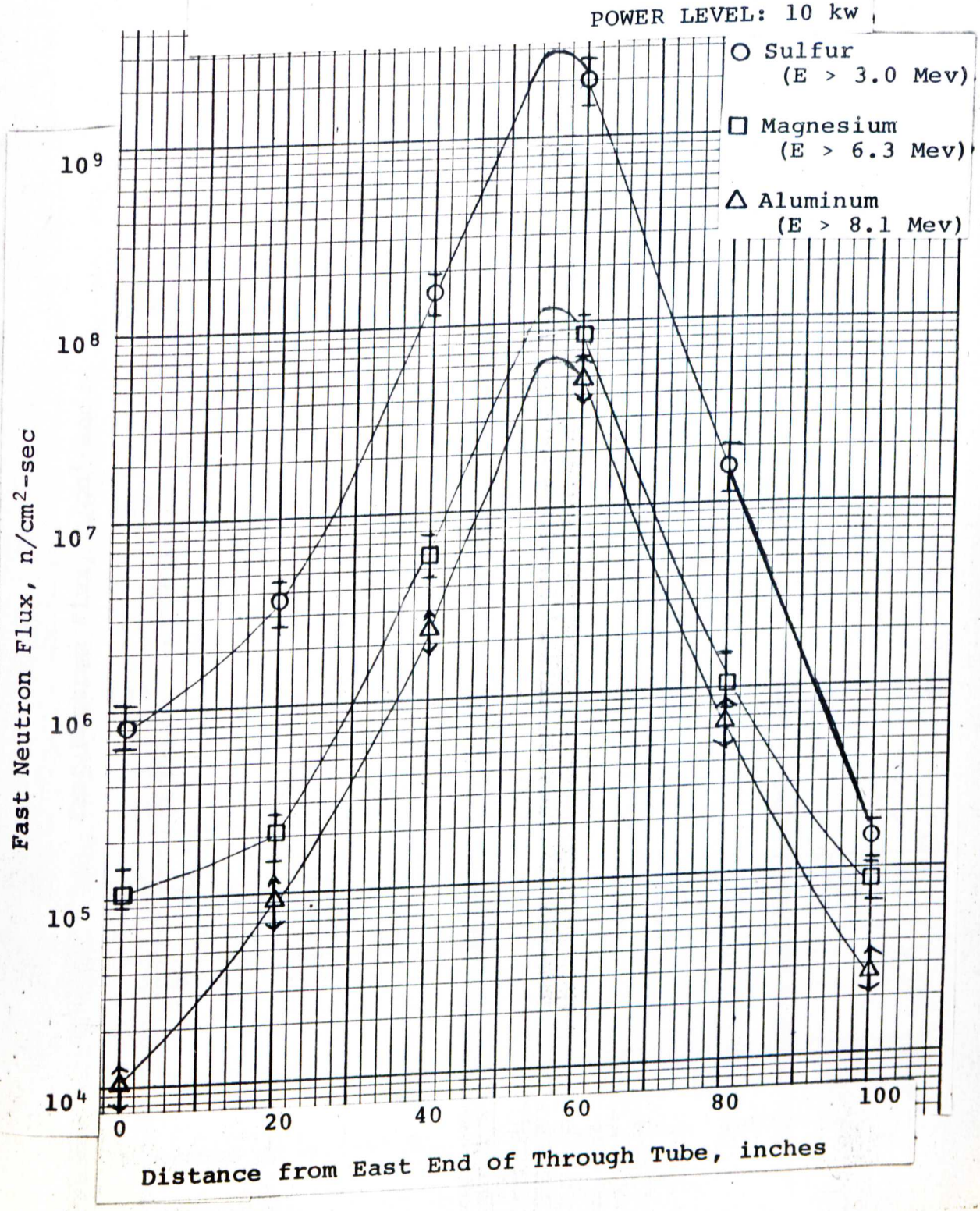

FIGURE 25

FAST NEUTRON FLUX DISTRIBUTION

ADJACENT TO NORTH WALL OF THROUGH TUBE

POWER LEVEL: 10 kw

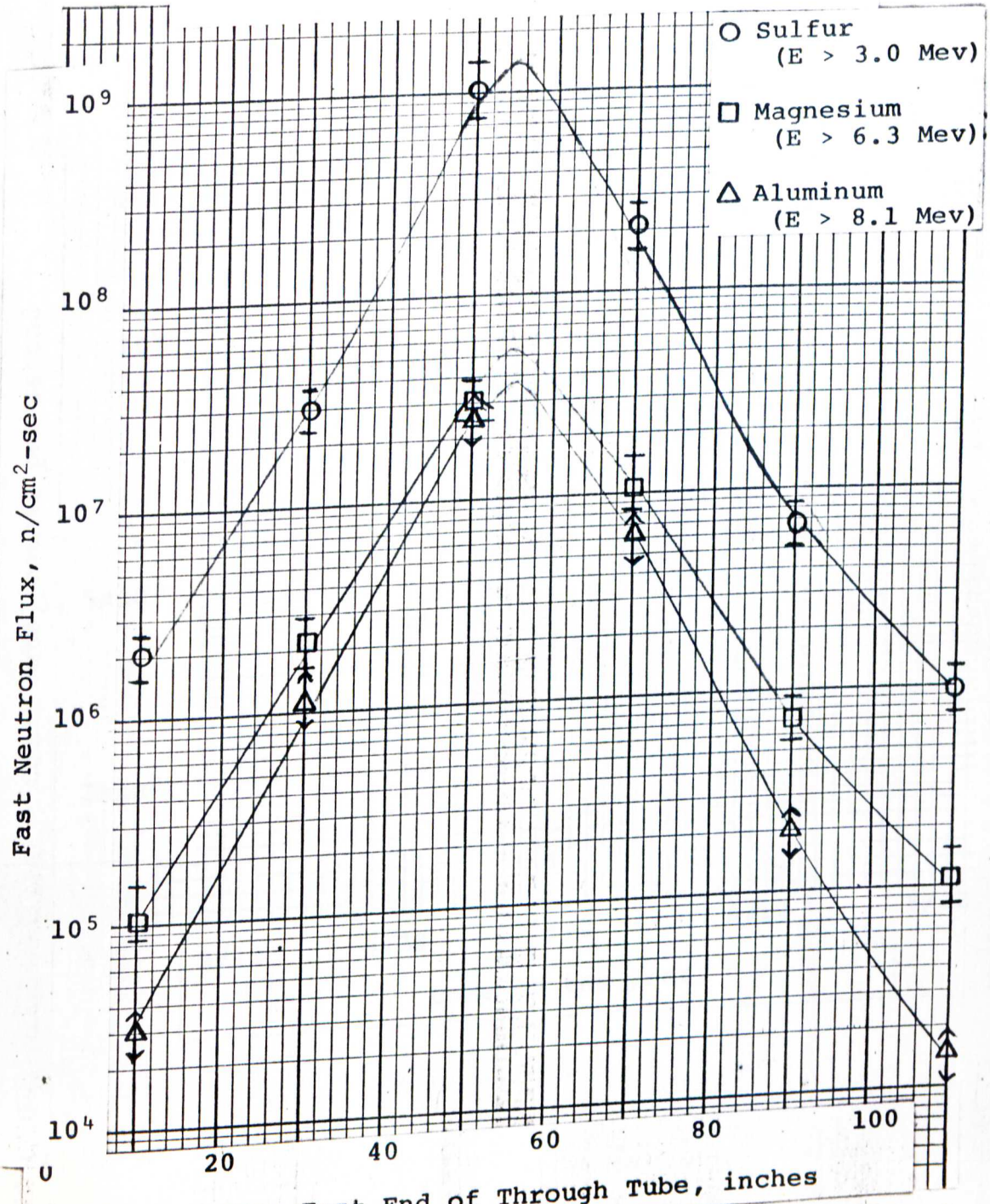

FIGURE 26

DECAY OF PHOSPHOROUS-32 IN A SULFUR MATRIX

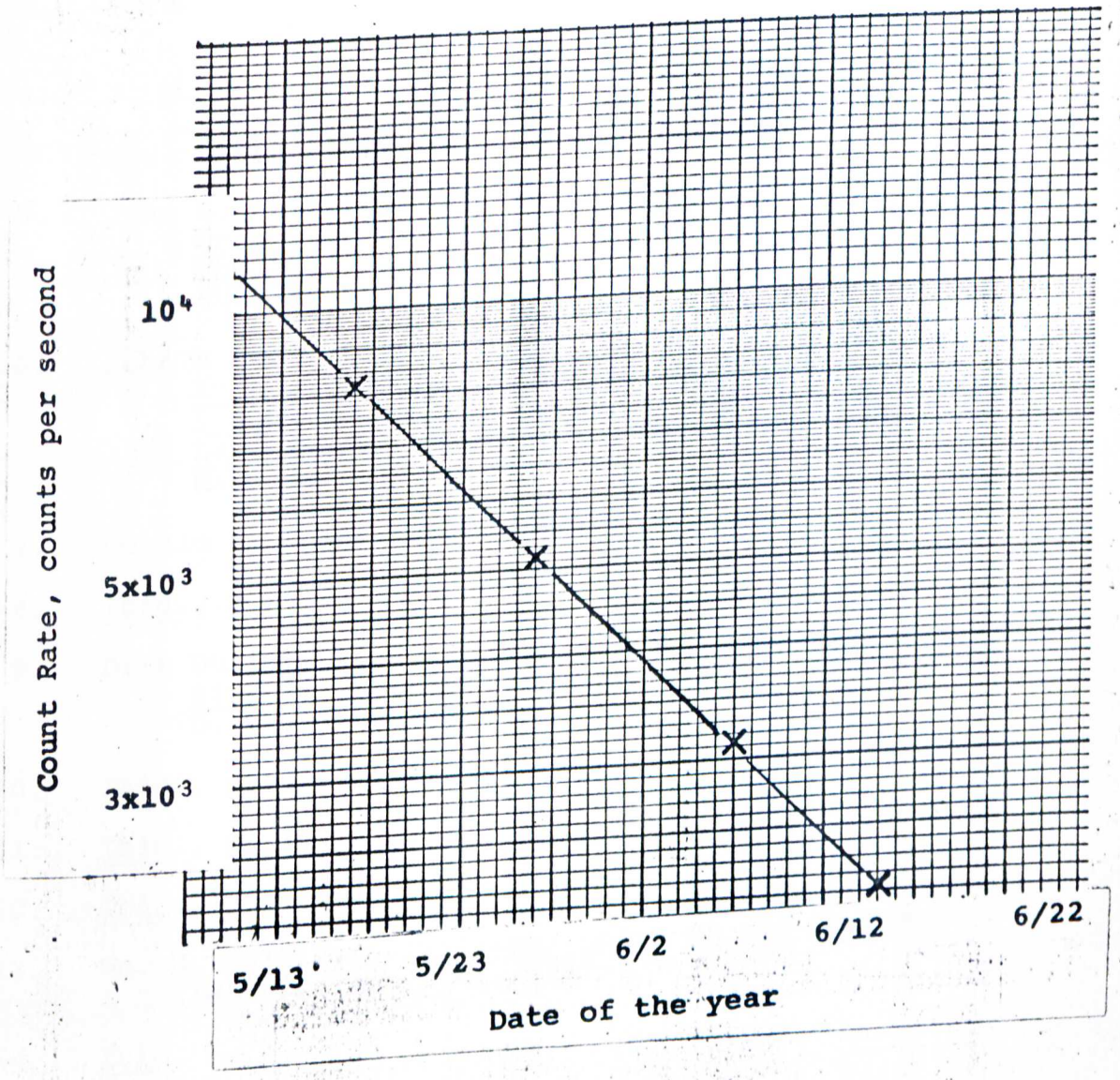

REFERENCES FROM THE TEXT

1. James Cermak, Master of Science Thesis, (University of Maryland, 1962)

2. Donald A. Lampe, Master of Science Thesis, (University of Maryland, 1964)

3. Gerald J. Hine and Gordon L. Brownell, Radiation Dosimetry, (New York, 1956), p.684

4. J. W. Kinch and D. L. Rigotti, An Activation Type Neutron Detection System and Its Calibration, #CWLR-2282, (Army Chemical Center, Maryland, 1956) (C)

5. John H. Mc Neilly, et al., Experimental Determination of the Reaction Cross Section for Mg^{24} $(n,p)Na^{24}$ and Al^{27} $(n,\alpha)Na^{24}$ at Several Different Energies, #NDL-TR-29 (Edgewood Arsenal, Maryland, 1962) (U)

6. John H. Mc Neilly and J. W. Kinch, Recent Developments in the Neutron Activation Threshold Detector System as Used by the U. S. Army Nuclear Defense Laboratory, #NDL-TR-15, (Army Chemical Center, Maryland, 1961) (U)

7. Donald A. Lampe, Section II

8. Ibid., Section II

9. Dick Duffey, et al., Safeguards Evaluation of the University of Maryland Reactor, #UMNE-1, (Washington, D. C., 1960), p.8

10. Ibid., p. 9

11. Ibid., p. 10

12. Ibid., pp. 12-19

13. Wm. H. Sullivan, Trilinear Chart of the Nuclides, (Washington, D.C., 1957)

14. Ibid.

15. Ibid.

16. Ibid.

17. Ibid.

18. Samuel Glasstone, Principles of Nuclear Reactor Engineering, (New York, 1955), pp. 126-128

19. Wm. H. Sullivan

20. J. W. Kinch and D. L. Rigotti

21. Ibid.

22. Dick Duffey, et al., p. 23

23. Philip G. Berman, Radiation Fields in Experimental Areas of the HDL-DORF Reactor, (in press)

A-1. Wm. H. Sullivan

A-2. Ibid.

B-1. Donald A. Lampe, Appendix C

B-2. Ibid.

C-1. Samuel Glasstone, p. 231

C-2. Ibid., P. 95

C-3. Dick Duffey, et al., P. 23

F-1. H. Etherington, ed., Nuclear Engineering Handbook, (New York, 1958), p. 1-27

F-2. Ibid.

F-3. Ibid.

F-4. Private communication from Dr. J. Fischer, Allis-Chalmers Manufacturing Company

SELECTED BIBLIOGRAPHY

Berman, Philip G., Radiation Fields in Experimental Areas of the HDL-DORF Reactor, Harry Diamond Laboratories, Washington, D. C., 1965 (in press)

Cermak, James, Master of Science Thesis, University of Maryland, 1962

Duffey, Dick, et al., jointly with Allis-Chalmers Manufacturing Co., Safeguards Evaluation of the University of Maryland Reactor, #UMNE-1, February 7, 1960

Etherington, H., ed., Nuclear Engineering Handbook, Mc Graw-Hill Book Co., Inc., New York, 1958

Evans, R. D., The Atomic Nucleus, Mc Graw-Hill Book Co., Inc., New York, 1955

Friedlander, Gerhart and Joseph W. Kennedy, Nuclear and Radiochemistry, John Wiley and Sons, New York, 1955

Glasstone, S., and Milton C. Edlund, The Elements of Nuclear Reactor Theory, D. Van Nostrand, Inc., Princeton, New Jersey, 1952

Glasstone, Samuel, Principles of Nuclear Reactor Engineering, D. Van Nostrand, New York, 1955

Griffith, R., Harry Murphy and Donald Wood, Passive Dosimetry Analysis Techniques, SWC-TDR-62-107, Air Force Special Weapons Center, Kirtland Air Force Base, New Mexico, January, 1964 (U)

Hine, Gerald J., and Gordon L. Brownell, Radiation Dosimetry, Academic Press, Inc., New York, 1956

Kinch, J. W., and D. L. Rigotti, An Activation Type Neutron Detection System and Its Calibration, CWLR-2282, Chemical Warfare Laboratories, Army Chemical Center, Maryland, July, 1959 (C)

Kohler, A. D., An Improved Method of Neutron Spectroscopy Using Threshold Detectors, UCRL-11760, Lawrence Radiation Laboratory, Berkely, California, December, 1964 (U)

Lampe, Donald A., Master of Science Thesis, University of Maryland, 1964

Levine, S. H., et al., Neutron Spectrum Measurements for the Northrop Reactor, Technical Memorandum NSL-64-187, Northrop Space Laboratories, Hawthorne, July, 1964

SELECTED BIBLIOGRAPHY (continued)

Marion, J. and J. Fowler, ed., Fast Neutron Physics, Vol IV Part II - Theory, Interscience Publishers, New York, 1960

Mc Neilly, John H., and John W. Kinch, Recent Developments in the Neutron Activation Threshold Detector System as Used by the U. S. Army Nuclear Defense Laboratory, HDL-TR-15, Nuclear Defense Laboratory, Army Chemical Center, Maryland, October, 1961 (U)

Mc Neilly, John H., et al., Experimental Determination of the Reaction Cross Sections for Mg^{24} (n,p) Na^{24} and Al^{27} (n,α) Na^{24} at Several Different Neutron Energies, Nuclear Defense Laboratory, Army Chemical Center, Edgewood, Maryland, April, 1962 (U)

Segre, Emilio, ed., Experimental Nuclear Physics, Vol II, John Wiley and Sons, Inc., New York

Sullivan, Wm. H., Trilinear Chart of the Nuclides, U. S. Government Printing Office, Washington, D. C., August, 1961

Whyte, G. N., Principles of Radiation Dosimetry, John Wiley and Sons, Inc., New York, 1959